QATAR UNIVERSITY

COLLEGE OF ENGINEERING

PREDICTION OF OPTIMAL HEXAGONAL INTERIOR ANGLE FOR ENERGY ABSORPTION: ANN TO PREDICT IN-BETWEEN EXPERIMENTAL DATA

BY

SHADA BENNBAIA

A Thesis Submitted to

the College of Engineering

in Partial Fulfillment of the Requirements for the Degree of

Masters of Science in Mechanical Engineering

June 2021

COMMITTEE PAGE

The members of the Committee approve the Thesis of
Shada Bennbaia defended on 19/04/2021.

_____
Prod. Elsadig Mahdi
Thesis/Dissertation Supervisor

_____
Jamil Renno
Committee Member

_____
Risby Mohd Sohami
Committee Member

Approved:

_____
Khalid Kamal Naji, Dean, College of Engineering

ABSTRACT

Bennbaia, Shada, T., Masters: June : 2021, Masters of Science in Mechanical Engineering

Title: Prediction of Optimal Hexagonal Interior Angle For Energy Absorption: ANN to Predict In-between Experimental Data

Supervisor of Thesis: Prof. Elsadig, S, Mahdi.

This thesis's proposed strategic procedure is to predict the interior angle of a hexagonal passive energy absorber structure based on specific properties using an ANN model, which has a great potential to be used as an intelligent engineering design tool. The application of passive energy absorption structures are continuously growing in automobiles, aerospace, packaging industries, and many more due to their high energy-absorbing capabilities. This study investigated the energy absorption performance of the aluminum hexagonal structure under quasi-static axial compression tests. These hexagonal structures are designed to have varying interior angle values to study their crushing behavior and identify the relationship between the energy absorption capability and the angle. Artificial Neural Network (ANN) model has been developed, optimized, and evaluated based on the Mean Squared Error (MSE) as a loss function to evaluate the performance of the model. During training, the configured ANN model had a training loss of only 0.09. The model predicted the hexagonal ring angle from unseen data with accuracy between 98.24% and 99.85%. Moreover, the predictive model was used to predict an optimal angle for targeted energy absorption properties based on two different cases. The

first case was to maximize the energy absorption and the crushing stability, while the second case was to maximize the load-carrying capacity and amount of energy absorption.

DEDICATION

I dedicate this work to my family for their continued support and motivation throughout this journey.

ACKNOWLEDGMENTS

"I would like to acknowledge the support of Qatar University for providing all the needs to achieve the requirements of this study."

TABLE OF CONTENTS

DEDICATION v

ACKNOWLEDGMENTS vi

LIST OF TABLES x

LIST OF FIGURES xi

CHAPTER 1: Introduction 1

1.1. Background Study 1

1.2. Project Objectives 4

1.3. Thesis Layout 4

CHAPTER 2. Literature Review 6

2.1. Energy Absorption Capability 6

2.2. Collapsible Energy Absorbers Under Lateral Loading 7

2.3. Metallic Energy Absorbers 12

2.3.1. Aluminum Energy Absorbers 12

2.3.2. Hexagonal Tubular Device 13

2.4. In-plane Quasi-Static Compression Test 15

2.5. Quantitative Energy Absorption Performance Indicators 17

2.5.1. Energy Absorption and Specific Energy Absorption 18

2.5.2. Initial Peak Force 19
2.5.3. Mean Crushing Force 19
2.5.4. Crushing Force Efficiency 19
2.6. Artificial Neural Networks 20
2.6.1. Artificial Neural Network for Engineering Design 20
2.6.2. Artificial Neural Network Architecture 21
2.6.3. Energy Absorption Predictions by Artificial Neural Network 23
CHAPTER 3. Experimental Study 25
3.1. Methodology 25
3.1.1. Fabrication Process 25
3.1.2. In-plane Quasi-Static Compression Test 27
3.2. Experimental Work Results and Discussions 29
3.2.1. Load-Displacement Curves Analysis 29
3.2.2. Energy Absorption Performance Indicators 45
CHAPTER 4. Artificial Neural Network 49
4.1. Methodology 49
4.2. Data Preprocessing 49
4.1.1. Model Development 51
4.1.2. Building and Training the ANN Prediction Model 53
4.1.3. Model validation 56
4.2. Models results and discussion 57

4.2.1. Model Performance 57

4.2.1. Angle Predictions 60

CHAPTER 5. Conclusion and Recommendations 62

5.1. Conclusion 62

5.2. Recommendations for Future Work 64

References 65

LIST OF TABLES

Table 1. Quantitative Energy Absorption Performance Indicators. 48

Table 2. Hexagon's Angles Ranking Based on Energy Absorption Performance 48

Table 3. The optimum configuration of the ANN model 56

Table 4. Four runs for predicting the angles using properties from the validation dataset59

Table 5. The associated losses and R^2 for each prediction run 59

Table 6. Prediction of optimal angle for energy absorption 61

Table 7. Prediction of optimal angle for load-carrying capacity 61

LIST OF FIGURES

Figure 1. Schematic of the (a) dumbbell-shaped novel tube, (b) cross-sectional view, and (c) self-locking tube. Reprinted with permission from [40]. 9

Figure 2. Nested tubular structures with the same outer circular tube and different inner structures (a) An oblong cross-section, (b) Two circular tubes with different diameters, and (c) two circular tubes with the same diameter [41]. 10

Figure 3. Collapsing history of the composite hexagonal system [45].....10

Figure 4. Honeycomb graded structure under in-plane quasi-static test [46] 11

Figure 5. Triangular multi-cell lattice structures under lateral loading [47].....12

Figure 6. Metallic hexagonal energy absorbers. a) Hexagonal metal columns under lateral loading [60]. B) Multi (upper) and single (lower) hexagonal tubes tested under axial loads [28]. c) Single-cell (upper) and hierarchical (lower) hexagonal tubes [62].....16

Figure 7. In-plane quasi-static test of a specimen that will be compressed. 17

Figure 8. Typical load-displacement curves with notations showing some of the essential EA indicators [71].....18

Figure 9. Test Specimen critical parameters dimensions.....25

Figure 10. Test specimens after fabrication.....26

Figure 11. Quasi-static compression test. a) Schematic representation of the loading condition. b) Test specimen in the INSTRON material testing machine 27

Figure 12. Pre-crush, post-crushing, and material densification phases of 40° sample 28

Figure 13. Load displacement curve for in-plane compression test of 30° hexagon and corresponding through test images. 31

Figure 14. Load displacement curve for in-plane compression test of 35° hexagon and corresponding through test images. 32
Figure 15. Load displacement curve for in-plane compression test of 40° hexagon and corresponding through test images. 33
Figure 16. Load displacement curve for in-plane compression test of 45° hexagon and corresponding through test images. 34
Figure 17. Load displacement curve for in-plane compression test of 50° hexagon and corresponding through test images 35
Figure 18. Load displacement curve for in-plane compression test of 55° hexagon and corresponding through test images. 36
Figure 19. Load displacement curve for in-plane compression test of 60° hexagon and corresponding through test images. 37
Figure 20. Load displacement curve for in-plane compression test of 65° hexagon and corresponding through test images. 38
Figure 21. Load displacement curve for in-plane compression test of 70° hexagon and corresponding through test images. 39
Figure 22. Load displacement curve for in-plane compression test of 75° hexagon and corresponding through test images. 40
Figure 23. Load displacement curve for in-plane compression test of 80° hexagon and corresponding through test images. 41
Figure 24. Load displacement curve for in-plane compression test of 85° hexagon and corresponding through test images. 42

Figure 25. Load displacement curve for in-plane compression test of the hexagons with angles from 30° to 50°. 43
Figure 26. Load displacement curve for in-plane compression test of the hexagons with angles from 55° to 85° 44
Figure 27. Plots of the independent variable against the dependent variable. 50
Figure 28. Strategic steps for ANN model development and prediction 52
Figure 29. The layered structure of the ANN predictive model 54

CHAPTER 1: INTRODUCTION

This chapter contains a brief introduction to the investigated problem, detailed objectives, and the general outline of this thesis.

1.1. Background Study

The hexagonal, circular, and square geometries are the most common metallic structures that have been investigated by researchers for their energy absorption capabilities [1, 2]. Their application of these protective structures is continuously growing in automobiles, aerospace, railway vehicles, packaging industries, and many more due to their high energy-absorbing capabilities. Aluminum is a lightweight metal that is widely used in the transport industry and several other industrial sectors due to its high-energy absorbability, combined with great bending stiffness and strength [3]. For that reason, aluminum-based crash energy absorbers have become more predominant in the vehicles' passive safety systems [4, 5]. The metallic passive energy absorbers are made of structures that can deform and collapse in a controlled behavior and dissipate impact energy in order to increase the passenger's safety and decrease the damage in the critical components of the vehicle [1, 6].

Over the past decades, studies have been conducted on the axial crushing of different cross-sections, such as the circular tubes, where they offer good energy absorption capability [7]. Other cross-sections that were extensively investigated are the polygons, especially the square, hexagon, and star geometries which also proved to have good energy absorptions under axial compression loads [8, 9]. However, limited studies investigated the effect of the interior geometrical parameters such as wall thickness, side lengths, and interior angles on the energy absorption capabilities and the energy absorbers' crush

behavior. Baykasoglu and Cetin [3] studied the effect of varying the wall thickness on aluminum-based circular tubes' energy absorption characteristics under axial impact loading. They concluded that the crashworthiness performance could be controlled and improved with the appropriate selection of the tubes' geometric parameters. Gowid et a., [10] investigated the use of a composite hexagonal quadruple ring system as a passive energy absorber device and found, through experiments, that the energy absorption capacity of this system significantly varies based on the interior hexagonal ring angle value. Therefore, it is proven that the geometry and the thickness are both factors that affect the structure's performance in terms of energy absorption.

Up-to-date, the study of energy absorption and quasi-static crushing behavior is done experimentally and numerically. Experimentally through performing experimental tests such as the quasi-static compression test, the results are analyzed through visual inspections throughout and after the test and from the load-displacement curves to calculate the quantitative energy absorption performance indicators discussed later. Numerical studies are mainly performed using finite element analysis software such as LS-DYNA to simulate the test and generate predictions of the energy absorption performance [11–13]. Regardless of the good agreement between the finite element analysis and the literature's experimental results, the authors noticed that the imperfections from the structures' fabrication process can not be included in the finite element analysis. One method to include the material inhomogeneity and specimen irregularities in the model is to use the experiments' results to predict the behavior of energy absorption structure with different geometrical parameters under loading. Artificial neural networks (ANN) is a machine learning tool that can use experimental data to predict energy absorption performance.

Using this artificial intelligence technique, any mperfections due to fabrication process are implicitly included within the neural network's input data.

ANN is one of the common machine learning algorithms, and nowadays, it is gaining more confidence to solve complex problems in science, business, and engineering applications [14–21]. ANN process information is inspired by how the biological nervous systems work and how the human brain processes and analyzes information. For that reason, ANN can effectively solve real-life non-linear problems that cannot be solved by classical programming. ANN has been used widely in diversified areas because of its unique features, such as its ability to learn and model complex and non-linear relationships. It does not impose any restrictions on the input variables; it provides fast learning with high accuracy for data classifications and value-based predictions and predicting future events from unseen data [22].

ANN model reliability is based on how the model architecture is formulated and constructed. The capability of predicting unseen values evaluates the performance. Thus, the ANN model's efficient and strategic construction can facilitate its use in diverse field applications. Intelligent product design can be achieved by utilizing ANN, especially where the relationship between the designing parameters can be established, facilitating the designing phase and allowing researchers to explore untapped intelligent design concepts by using advanced predictive models.

Conducting a series of experiments requires extra cost and time. These experiments are necessary to reach a high level of understanding of the specific subject. In this case, the main objective is to predict an optimal hexagonal ring angle through the structure energy absorption (EA) capability and mechanical properties, while there no direct

correlation between these properties and the hexagonal ring interior angle. If the optimal geometry parameter can be determined with a predictive model's help, experimental work can be designed to be more time-efficient and cost-effective. However, the use of ANN predictive models trained on experimental data for predicting aluminum hexagonal ring interior angle has not been addressed in the literature.

This work proposes a systematic approach for determining the optimal interior angle of a hexagonal ring for energy absorption applications using ANN models. The model will be developed to predict the targeted angle to optimize the energy absorption capabilities. The approach used to develop the ANN model in this work can be extended for other geometrical parameters and cross-sections if the necessary experimental data are available.

1.2. Project Objectives

1. To investigate the influence of changing the interior angle of a hexagonal ring structure on its energy absorption capability under in-plane quasi-static loading.
2. To build and validate an ANN predictive model that can predict and optimize the interior angle of a hexagonal ring based on desired energy absorption performance with an accuracy higher than 90%.

a. Thesis Layout

This thesis is divided into five chapters. The next chapter, Chapter 2, is the literature review from related sources regarding the behavior of energy absorption capabilities, collapsible metallic energy absorption devices, in-plane quasi-static crushing of metallic

tubular devices, the quantitative energy absorption performance indicators, artificial intelligence in mechanical design, and predictions by ANN models. Chapter 3 presents the experimental study astarting from a systematic and detailed description of the methodology used to fabricate the test specimens and conduct in-plane quasi-static compression tests to the results and discussion of the experimental work. In Chapter 4, the methodology of artificial neural network predictive model development and training is presented, followed by the predictions results and detailed discussion. Lastly, Chapter 5. presents the conclusion and recommendations for future work.

CHAPTER 2. LITERATURE REVIEW

In this chapter, the literature related to similar work was reviewed. Accordingly, information is given on energy absorption capability, collapsible energy absorbers under lateral loading, energy absorbers made of aluminum, and hexagonal energy absorbers. The in-plane quasi-static test was explained, and quantitative energy absorption performance indicators were presented in detail. Furthermore, previous work concerning artificial neural networks in engineering design and specifically in energy absorbers design was reviewed.

2.1. Energy Absorption Capability

Researchers and engineers and are continuously attempting to develop efficient structures for energy absorption. These structures are essential, especially in automobiles, where they are used in vehicles to absorb collision energy to avoid or minimize any damage to the passengers or the critical components such as the motor. When the energy absorbers plastically deform, they dissipate the impact kinetic energy. The geometry and material are important aspects to consider when developing an efficient energy-absorbing component [23].

The energy absorbed by a structure can be measured by calculating the area under the load-displacement curve that can be obtained from a quasi-static test. Energy absorption capability can be described and measured by the specific energy absorption (SEA), where it can be measured by dividing the total energy absorbed over the structure's unit mass. The initial peak force and the mean force the structure experience when absorbing energy are two of the primary energy absorption capability indicators [24]. The load-deformation curve is also used to measure the crashworthiness of the energy absorber [25]. The

crashworthiness is the capability of materials to fail within controlled modes and mechanisms during absorbing impact energy while keeping stable load deterioration [26].

According to Mahdi et al. [27], crushing capability can be described through 3 phases. The first phase represents the total energy absorbed during the pre-crush phase until the initial peak force. The second phase is the total energy absorbed in the post-crash zone, and the third phase is the total energy absorbed in the material densification phase. The energy absorbed in the third phase is negligible as it is usually trivial.

2.2. Collapsible energy absorbers Under Lateral Loading

It is important to observe how a structure can absorb impact energy through collapsing and deforming itself. The characteristics of structure deformation predict its ability, i.e., the structure may or may not be appropriate for a certain application. Collapsible structures such as tubes, columns, and honeycombs can absorb energy when subjected to loadings, where the absorbed energy dissipates through different failure mechanisms [28]. Alexander [29] was the first to use these structures as energy absorbers after investigating the in-plane loading for cylinders. Tubular structure folding is one of the common mechanisms that provide energy absorption capability. Subsequently, Abramowicz and Wierzbicki [30], Abramowicz and Jones [31] and, Andrews et al. [32] carried out theoretical and experimental studies on tubular collapsible structures with different cross-sections, such as circular, square and hexagonal, by subjecting these structures under quasi-static loading. Gupta and Abbas [33] also conducted an experimental study of composite cylindrical tubes under quasi-static lateral compressing

Alghamdi [34] conducted a study to review collapsible energy absorbers with

different shapes and different deformation mechanisms under loading. Examples of these shapes are square tubes, circular tubes, honeycombs, and sandwich plates. The deformation modes reviewed include lateral flattening, lateral indentation, axial crushing, inversion, and splitting.

Lateral flattening of is the deformation mode studied in this work. It founded that in tubular structures, the amount of plastic deformation was most global in the axial crushing, then in lateral flatting then in the lateral indentation. Deruntz and Hodge [35] analyzed the plastic deformation of a single tube under lateral compression. Furthermore, Reddy and Reid [36] studied the lateral compression of tubular energy absorbers supported by side constraints; the results showed that the energy absorbed by a constrained system increased by 300% compared to an unconstrained system. Wu and Carney [37] investigated the initial collapse of braced elliptical tubes and found that the energy dissipation increased when the elliptic tubes are crushed along their major axes. Mahdi and Kadi [38] presented a study investigating the composite elliptical tubes crushing behavior under lateral compression test and found that the ellipticity ratio has a significant effect on the crushing behavior of the loaded tubes.

The design of tubular structures under lateral loading needs to be enhanced to improve energy absorption capability and crashworthiness properties as they showed ineffective performance when absorbing impact energy [39]. To improve energy absorption under lateral loading, Chen et al. [40] designed a novel self-locked device with a dumbbell shape shown in Figure 1; mild steel is used to fabricate this structure. During compression, the interlocked design provides a lateral constraint. The authors used this

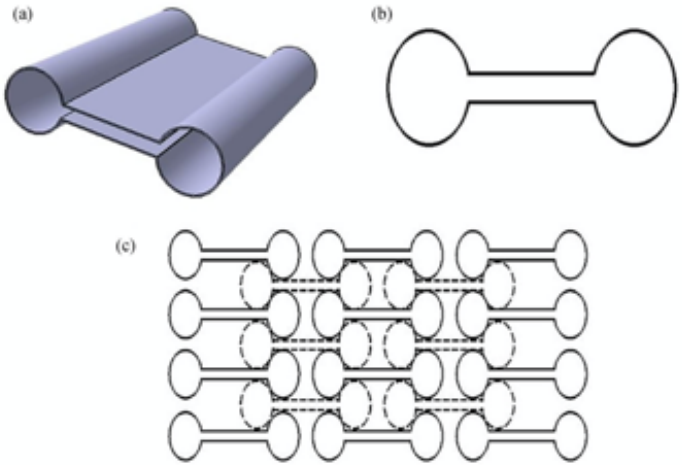

Figure 1. Schematic of the (a) dumbbell-shaped novel tube, (b) cross-sectional view, and (c) self-locking tube. Reprinted with permission from [40].

stacking arrangement and the dumbbell-shaped energy absorber geometry to prevent tubes splashing when a circular tube is used with the same arrangement.

Many researchers [39–42] have investigated the capability of stacked systems to absorb impact energy. Nested or stacked systems are customarily designed for a particular application with a defined stroke length. It is easier to design nested tubular structures in comparison to design multi-cell structures. A nested tube is defined as a tube with multiple energy-absorbing elements, in the same system and compared to a single tube, the nested system provides higher EA capability per unit length [41]. Baroutaji et al. [41] conducted a parametric study on nested tubular structures to examine their EA performance under lateral dynamic and quasi-static loadings. Three types of the studies nested tubular systems are illustrated in Figure 2; they consist of oblong and circular tubes. Results showed that the systems showed a similar response in the load-displacement curve under dynamic and quasi-static loadings.

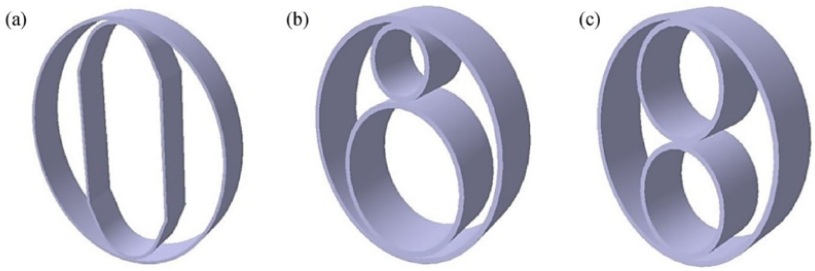

Figure 2. Nested tubular structures with the same outer circular tube and different inner structures (a) An oblong cross-section, (b) Two circular tubes with different diameters, and (c) two circular tubes with the same diameter [41].

Mahdi et al. [45] experimentally investigated composite hexagonal ring systems' crushing under in-plane quasi-static loading. They discovered that the hexagonal ring geometry (e.g., angle and side lengths) significantly affects energy absorption capability and the failure mechanism. Figure 3 shows the collapsing history of the hexagonal ring system.

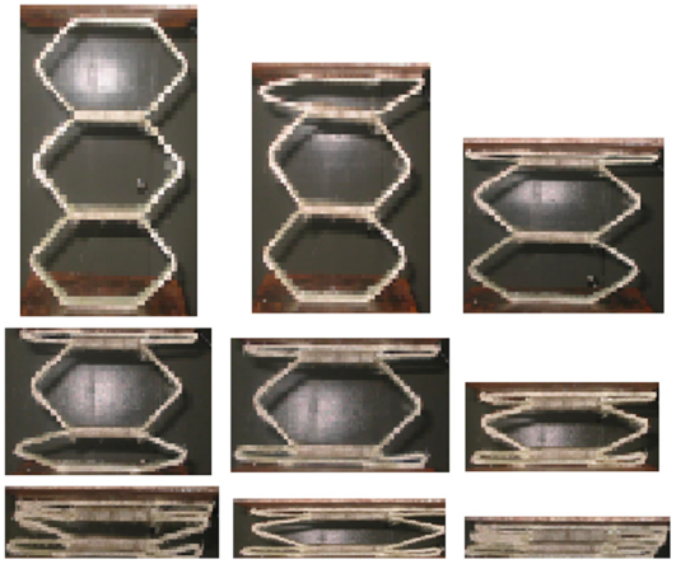

Figure 3. Collapsing history of the composite hexagonal system [45]

Galehdari et al. [46] studied a graded honeycomb structure (Figure 4) as a lightweight energy absorber and analyzed its crushing behavior under in-plane quasi-static and low-velocity impact loading. The research objective was to create an analytical model that can be used to study this structure. The obtained results from the analytical model showed good compliance with the experimental results.

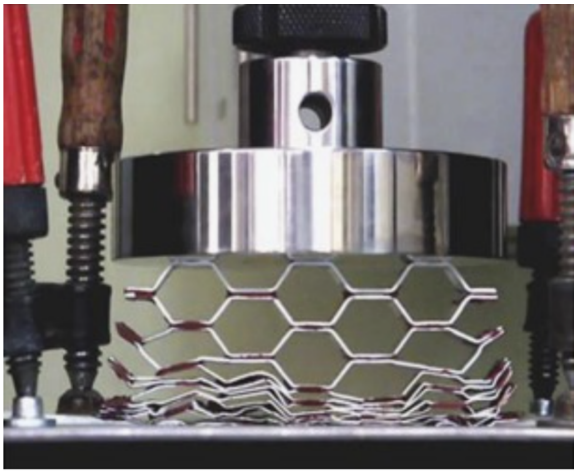

Figure 4. Honeycomb graded structure under in-plane quasi-static test [46]

Sun et al. [47] carried out an in-plane compression test for a triangular multi-cell lattice structure to investigate its collapsing mechanisms and folding modes. As shown in Figure 5, the crushing started from the top layer under compressive loading then gradually progressed to the below layers. From the load-displacement curve, they found that there are three stages of deformation mode for each layer. Similarly, collapsing of a single triangle has the same deformation mode. This study's multi-cell structure provides better energy absorption with lower initial peak force compared to a single triangular structure.

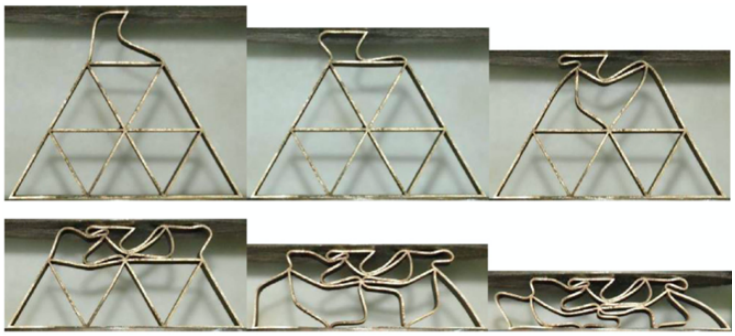

Figure 5. Triangular multi-cell lattice structures under lateral loading [47]

Advanced tubular energy absorbers derived from common structures exhibit good EA performance under axial loading from reviewing the available literature. However, studies on the response of these structures under lateral loading conditions remain very limited. Thus, more studies should be conducted to furtherly explore the performance and deformation mechanisms under lateral loading.

2.3. Metallic Energy Absorbers

2.3.1. Aluminum Energy Absorbers

Throughout the years, researchers explored the collapse mechanisms of lightweight metallic structures. Most of the studies focus on axial loading conditions. Aluminum is a lightweight metal that has seen increased use in automobiles as a replacement for steel. The benefits the lightweight metallic materials can provide made them attractive to the automobile industry. Using aluminum instead of conventional steel in vehicle structures can save up to 25% by reducing fuel consumption and carbon dioxide emissions[48].

The design of aluminum structures and the study of crashworthiness have been extensively investigated [48–56]. Demirci and Yildiz [57] compared thin-walled energy

absorbers made of different types of steel, magnesium alloys, and aluminum alloy in crush performance and EA capability to be used as lightweight structures in vehicles. They found that steel achieved better EA capability compared to magnesium and aluminum absorbers. However, aluminum provided a better capacity of AE absorption per unit mass.

Andrews et al. [32] experimentally studied aluminum tube's crushing behavior and classified the failure modes into four classes; diamond, concertina, bulking, and mixed. Li et al. [58] studied the lateral crushing behaviors of circular tubular structures made of aluminum, carbon fiber reinforced plastics, and glass fiber reinforced plastics. To study the effect of the structure's geometries, different configurations of thickness and diameter-to-thickness ratio are utilized. Because of the aluminum's ductile behavior, the aluminum tubes showed significantly greater lateral crashworthiness than the composite tubes. Furthermore, with the higher diameter-to-thickness ratio, aluminum tubes also provided better crashworthiness than composite tubes.

2.3.2. Hexagonal Tubular Device

Researchers have a growing interest in studying the plastic deformation of the metallic energy absorbers with hexagonal geometry and cross-section under lateral and axial and loadings. The structures with hexagonal cross-sections were proved to have superior crashworthiness due to their folding mechanism [59].

Rahmani and Abbas [60] used the hexagonal metal ring as energy absorbers and investigated their plastic deformation under lateral quasi-static loading (Figure 6, a). The specimens were made of different metals such as steel, galvanized iron, and brass alloy. They found that hexagonal column's crashworthiness is significantly affected by the column's length, wall thickness, and material properties. Several studies were investigating

hexagonal cellular structures to understand their crushing behavior. Alkbir et al. [61] studied a cellular structure consists of hexagonal cells with varying interior angles from 45° to 60° and concluded that as the angle increases, the SEA increase. Composite hexagonal ring systems with different angles from 45° to 70° were tested under in-plane quasi-static loading. The experimental results showed that the energy absorption capability increases as the system's angle increases; thus, angle 70° achieved the best energy absorption capability among all tested samples [38].

Xu et al. [59] proposed a unique hierarchical hexagonal column that showed an ability to enhance crashworthiness and EA performance. The hierarchical hexagonal columns structure is designed to have smaller hexagons at the corners of the central hexagon. This study's results open the door to a new route of designing new novel structures with high crashworthiness and EA absorption capacity.

Nia and Parsapour [28] have designed aluminum single and multi-cell thin-walled tubular structures with different cross-sections, such as triangular, hexagonal (Figure 6, b), square, and octagonal. These tubular structures were subjected to quasi-static loading to obtain experimental data that can validate numerical simulations. They concluded that the EA capability of multi-cell structures is better than the capability of single-cell sections. Furthermore, the hexagonal and octagonal cross-sections sections of a multi-cell configuration exhibited the best specific energy absorption.

A similar conclusion was reached by Li et al. [62] as they found that multi-cell metallic tubes provide more efficient specific energy absorption than single-cell tubes (Figure 6, c). They tested and analyzed two tubular structures, one has a hexagonal single-cell cross-section, and the other has a hierarchical multi-cell cross-section. Finite element

analyses and axial compression tests are used to investigate the crushing behavior of the structures. The results showed that the hierarchical tubes have three crushing mechanisms has three folding phases, sub-cell folding, mixed folding, and global folding. In the sub-cell folding mechanism, the mean crushing force is significantly increased, and the force reached its maximum when in the mixed folding phase, which is in between the sub-cell folding and global folding. Numerical models are built for these folding styles and used to predict the mean crushing force.

2.4. In-plane Quasi-static Compression Test

The quasi-static test is one of the most common tests used to study the structural performance, energy absorption capacity, and crashworthiness of structures [63–68]. In the quasi-static tests, the specimen is compressed between two steel plates at a very low speed by a hydraulic press (Figure 7). The sample under quasi-static testing is crushed at a steady rate using a universal testing machine. The test specimen is laterally or axially compressed, depends on the position and geometry of the structure between two flat steel plates positioned parallel to each other. The lower plate is kept static while the top plate moves downwards at a constant speed.

For crushing and energy absorption performance analysis, the quasi-static testing might not ideally replicate an actual crash condition. In an actual collision, the structure subjected to crushing loading does not experience a constant loading as the loading is maximum at the beginning if the collusion then starts to decrease until stopping.

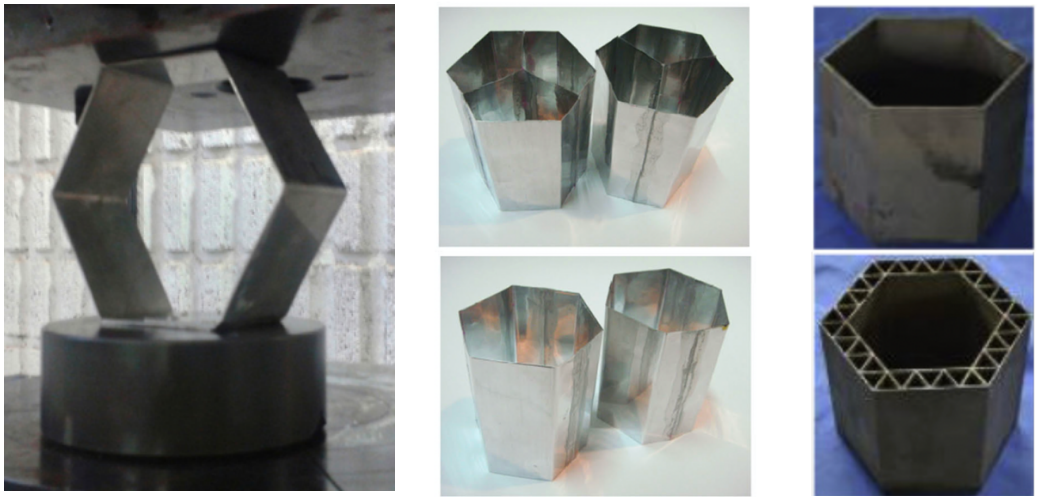

(a) (b) (c)

Figure 6. Metallic hexagonal energy absorbers. a) Hexagonal metal columns under lateral loading [60]. B) Multi (upper) and single (lower) hexagonal tubes tested under axial loads [28]. c) Single-cell (upper) and hierarchical (lower) hexagonal tubes [62].

However, to initiate a structural performance study of any structure, it is recommended to investigate the deformation styles and failing modes under a quasi-static load. For automobile applications, the tubular structures used as collapsible energy absorbers are mostly attached at one end, where the energy absorption and crushing start at the free end, which is a similar condition in the quasi-static crushing [69].

In quasi-static testing, it is relatively easy to control the test conditions. Usually, the test's required equipment is cheaper than the ones needed for impact testing due to the very high speed that should be used in impact testing. Thus, quasi-static testing provides a means to experimentally study the structures' failure mechanisms and EA capability at slow crushing speed. The machine used in the quasi-static test has a computerized data acquisition system that automatically recorded load-displacement curves. These curves are used to get an insight into the failure mechanisms, obtain, and calculate different parameters used to evaluate the tested structure's energy absorption capability.

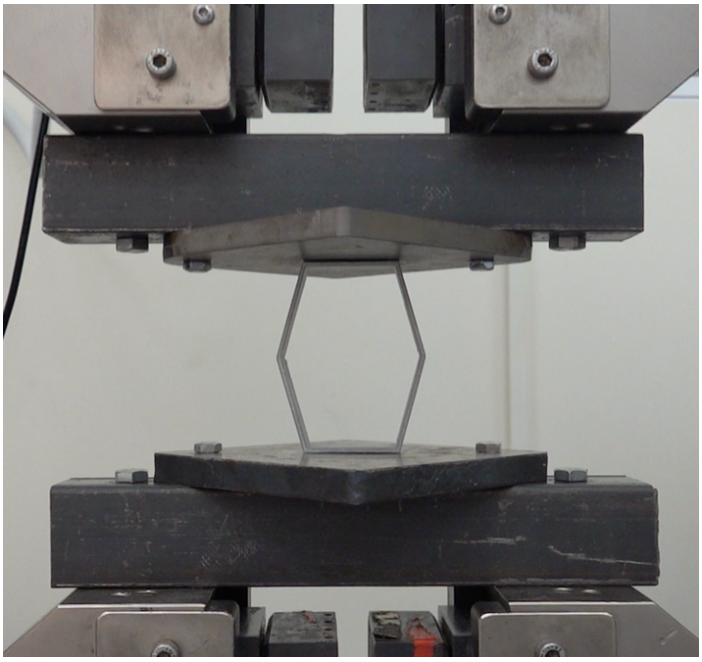

Figure 7. In-plane quasi-static test of a specimen that will be compressed.

2.5. Quantitative Energy Absorption Performance Indicators

Quantitative analysis of a structure's energy absorption capabilities requires quantifying the crashworthiness characteristics to enable the research to understand the structure's capabilities [70]. In this section, the Critical EA indicators used in this work are explained in detail. Figure 8 illustrates a typical load-displacement curve with notations showing some of the essential parameters used to obtain and calculate the EA performance indicators.

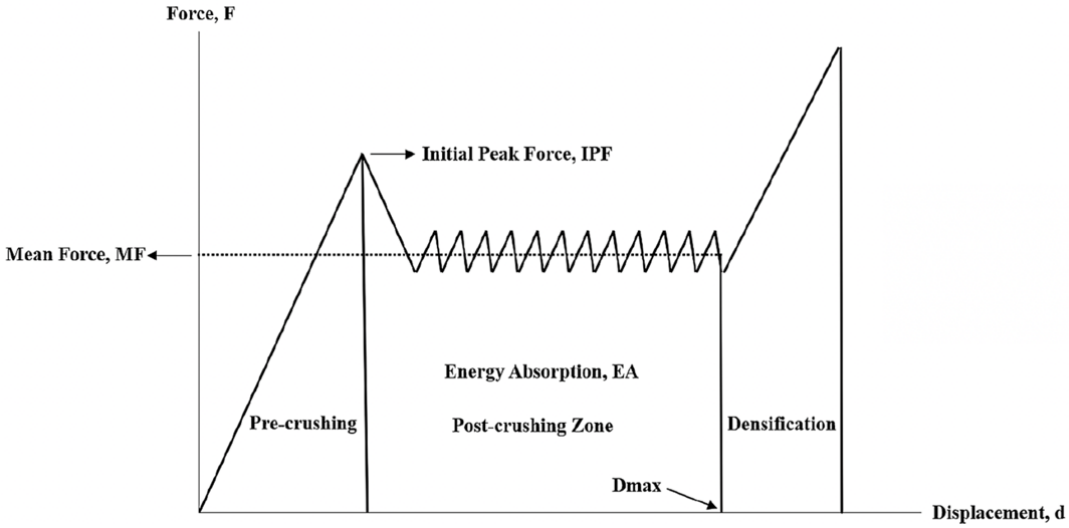

Figure 8. Typical load-displacement curves with notations showing some of the essential EA indicators [71]

2.5.1. Energy Absorption and Specific Energy Absorption

Energy absorption value is used to evaluate structures' ability to absorb crushing energy. The amount of absorbed energy can be determined by calculating the area under the load-displacement curve. It can be calculated by integrating the load (F) concerning the crushed height. The formula is as follows [72]:

$$EA = \int_0^{Dmax} F(s)\, ds \qquad 1$$

The specific energy absorption (SEA) is the energy absorbed per unit mass of the crushed structure [23].

$$SEA = \frac{EA}{m} \qquad 2$$

2.5.2. Initial Peak Force

The initial peak force (IPF) is the load required to start plastic deformation. To increase the crushing's stability and provide a better safety mechanism during collisions when the structure is used as an energy absorber in vehicles, it is recommended for the IPF to be lower to reduce the reaction forces experienced during collisions [23].

2.5.3. Mean Crushing Force

The mean crushing force (MF) is the average force that a structure is experiencing during the post-crushing Phase. The forces experienced in the densification stage are excluded when calculating the MF. The formula is as follows [70]:

$$MF = \frac{EA}{Dmax} \quad (3)$$

Where $Dmax$ is the displacement of the structure at the end of the post-crushing phase.

2.5.4. Crushing Force Efficiency

Crushing force efficiency (CFE) is the ratio of the mean crushing force to the initial peak crushing force [71]:

$$CFE = \frac{MF}{IPF} \quad (4)$$

It is preferred for the CFE to be close to 1 as this means the crushing behavior during the post-crushing phase is stable. CFE value of one means that the IPF is sustained throughout the entire post-crushing phase, and it is equal to the mean crushing force [71].

2.6. Artificial Neural Networks

2.6.1. Artificial Neural Network for Engineering Design

In engineering design, computers are essential in daily activities as engineers use many applications to enhance their designs. Engineers have utilized artificial intelligence (AI) to accomplish design tasks since the 1970s [73]. One of the most known AI applications is artificial neural networks (ANNs). Recently, they have been widely utilized in many fields of engineering and science. The late 80s is when early applications of ANN in are used in civil engineering [74]. ANNs are machine learning algorithms capable of performing advanced pattern recognition and fittings that enable users to obtain complex relationships between non-linear variables [75]. This learning process can occur even if the input data are incomplete, fuzzy, or contain errors, or is incomplete or fuzzy, which is how data usually are during the design process. ANNs can conduct different tasks, such as prediction, identification, filtering, and control. These features of ANNs make them a favorable candidate to model a variety of engineering problems [74].

The way the biological neurons inspire aNNs process information through neurons in the human brain. These algorithms are trying to replicate the human brain learning activities, except that they are simpler as they consist of fewer components and work abstractly.

The neural network's training process contains entering examples that learn the input dataset patterns, along with a known target output. The system modifies the weights of the network's internal connections to reduce the errors between the network's predicted output and target known output. After the ANN is trained and tested and proved satisfactory performance, it can generalize rules and use them to react to unseen input data to predict the output, which has to be within the training dataset domain.

Feedforward artificial neural networks are among the most used ANN algorithms in different applications due to their great success in solving the desired problems. The main advantage of ANNs is that they do not need an algorithm that is user-specified to solve a specific problem as the classic programming, as problem-solving, instead, like humans, they can learn through examples. Another advantage of the ANN is their generalization ability which indicates that they can identify and react to patterns similar to the patterns they have been trained on [76]

It is still a nontrivial task to build a perfect ANN, mainly due to difficulties finding the networks' architecture, which dramatically affects the ANN performance and accuracy [77].

2.6.2. Artificial Neural Network Architecture

The ANN architecture consists mainly of several hidden layers, hidden nodes, and connections between those nodes. If the ANN architecture is improperly built, it might cause the model to be overfitting, significantly reducing its accuracy.

One of the most common algorithms to train multilayer feedforward ANN is the backpropagation algorithm. It is composed of an input layer, many hidden layers, and an output layer. Backpropagation training provides a technique to fine-tune a neural network's

weights depending on the error obtained from the previous training iteration (i.e., epoch). Efficient weights tuning can reduce error and make the model more reliable by increasing its improved generalization [78].

Typically an ANN architecture consists of the following elements [76]:

1. The number input layer
2. The number of hidden layers.
3. The number output layer
4. The number of neurons in each layer
5. The number of epochs
6. The activation function of each layer
7. The training algorithm

Basically, o be able to feed and obtain data to and from an ANN, only the output and input layers are the minimum requirements. The number of neurons that should be in the input and output layers depends on the number of input and output variables of the model. Thus, the challenge is to determine how many hidden layers are required and how many neurons should each hidden layer contain. A higher number of hidden layers in ANN could improve the model's performance. For example, two hidden layers are more efficient for many types of non-linear problems than an ANN with only one hidden layer [18].

One of the typical methods used to determine ANN architecture is the trial-and-error method. In this method, different architectures are evaluated and compared to each other. This process can be time-consuming and involves high uncertainty as it mainly depends on the human expert's intuition and experience [76]. Srivastava et al. [79] used the

dropout method to determine the ANN structure and prevent overfitting. In this method, the ANN nodes are dropped out randomly to find the most accurate structure during the training process.

2.6.3. Energy Absorption Predictions by Artificial Neural Network

ANNs can be used as a technique that can be trained to predict a structure's behavior from existing experimental data. Caliskan [12] conducted one of the first published studies the utilizes ANNs in predicting the crushing behavior of composite structures based on input data from tensile properties. The study also predicted the amount of energy absorbed by circular tubes made of carbon fiber-reinforced under axial loading. He used a simple ANN with a backpropagation training algorithm and experimental data set of 84 rows of absorbed crushing energy by the tubular structures.

Mahdi and El-Kadi [19] used the ANN technique to predict the energy absorption characteristics and the crushing behavior of laterally loaded elliptical tubes made of glass fiber/epoxy composite. The predicted energy absorption capability and load-carrying capacity were compared to actual data from the experiment and showed good compliance. This indicated that ANN could be an effective tool in predicting collapsible composite energy absorbers' behavior when subjected to loading conditions.

Kazi et al. developed an ANN model to predict the optimal filler content in cotton fiber/polypropylene composite material for targeted mechanical properties. The ANN model was trained using existing experimental and built via Keras library in Python. The grid search method is used to tune the model's hyperparameter and k-fold cross-validation to achieve a good performing model capable of predicting reliable results for targeted filler

content. Using predictive models to predict a targeted material design parameter is proved to be efficient in reducing the time and effort used for material characterization.

Gowid et al. [10] also build ANN predictive model to predict the non-linear crushing behavior and the optimal angle for EA of a hexagonal quadruple ring system with different angle configurations made of composite material. Mean Square Error is used to estimate and optimize the model performance. The predicted results are compared to the actual results for experiments to evaluate the prediction's true error. The ANN model accurately predicted the energy absorption capability and load-carrying capacity for different angles where the reported mean square Error was 0.39 N and 1 J, respectively. The model was used to optimize the hexagonal ring system's angle to maximize the EA capabilities; the system's optimal angle was predicted to be 47° with 69 J of absorbed energy.

CHAPTER 3. EXPERIMENTAL STUDY

In this chapter, the methodology used to conduct the experimental study is described. The first section demonstrates the test specimens fabrication process, which is hexagonal structures with different internal angles—followed by presenting the in-plane quasi-static compression test conducted to study the structures crushing behavior and obtain the load-displacement data. The second section shows and explains the tests' detailed results by analyzing the resulting data, discussing and evaluating each hexagonal structure's energy absorption performance based on the calculated energy absorption indicators.

3.1. Methodology

3.1.1. Fabrication Process

In this study aluminum sheet with a thickness of 20 millimeters (mm) is used to fabricate the specimens. These specimens are hexagons with a thickness of 3 mm, a fixed height of 100 mm, fixed top and bottom sides length of 50 mm, and varying interior angle θ configurations from 30° to 85° with an increment of 5° (30°, 35°, 40°, 45°, 50°, 55°, 60°, 65°, 70°, 75°, 80°, 85°) as illustrated in Figure 9.

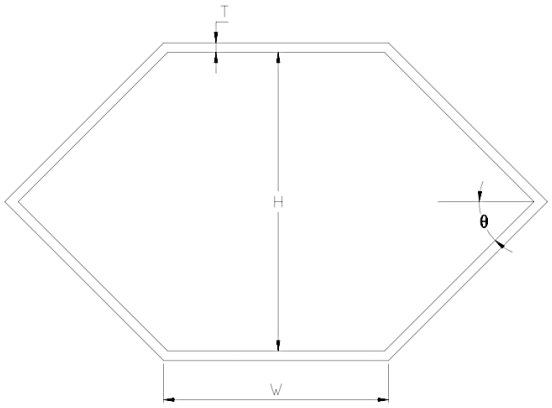

Figure 9. Test Specimen critical parameters dimensions

A water jet machine is used to cut the hexagonal specimens from the aluminum sheet. Three samples of each angle configuration are fabricated to be tested under a quasi-static compression test, as shown in Figure 10.

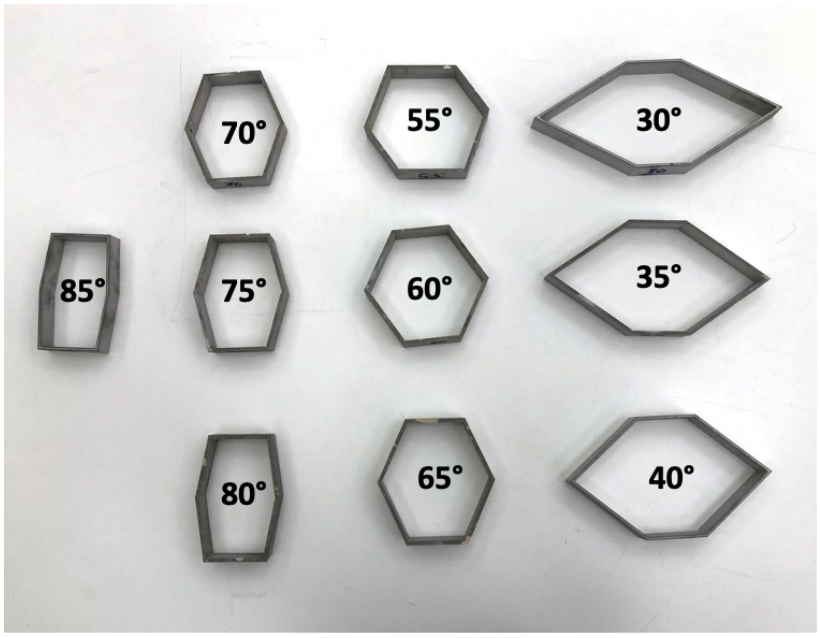

(a)

(b)

35°

55°

85°

(c)

Figure 10. (a) and (b): test specimens after fabrication (Note: Specimens with angles 45° and 50° are fabricated after the show specimens are tested). (c) Close-up shots for a few of the samples.

3.1.2. In-plane Quasi-Static Compression Test

Quasi-static crushing was carried out using the INSTRON material testing machine. The test machine has two plates where the specimen is placed in between them. The lower plate was kept stationary while the upper plate was positioned to contact the test sample's upper surface as it will be moving downwards at a constant speed to apply the load during the test see Figure 11. The same loading conditions were applied to all specimens, compressed at a 10 mm/min speed up to a displacement of 90 mm to collect around 5500 data points to build an accurate load-displacement curve for each test. The machine computerized data acquisition system automatically records Load-displacement curves during testing. The crushing process for all specimens under compressive loading was recorded in high-quality videos to provide a detailed crushing process's history to observe and analyze the crushing mechanisms.

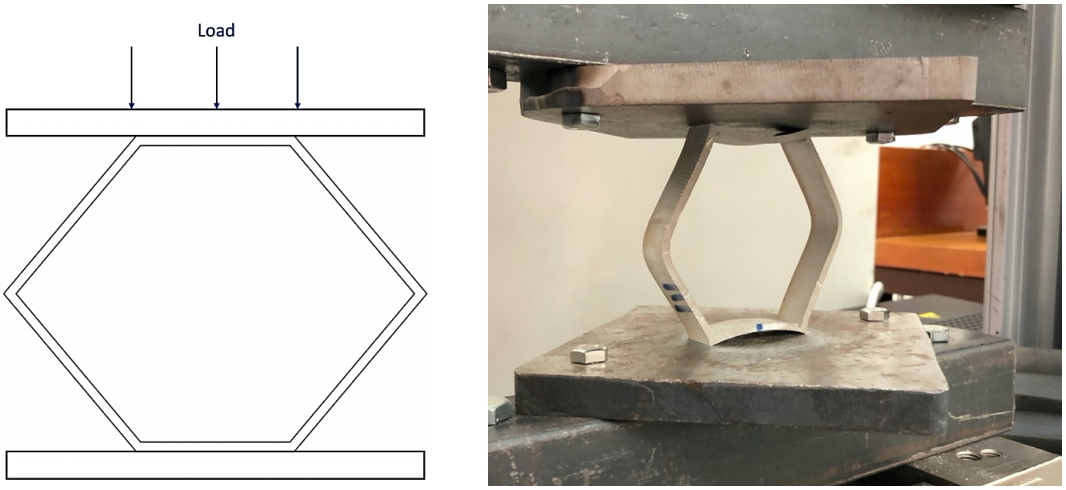

(a) (b)

Figure 11. Quasi-static compression test. a) Schematic representation of the loading condition. b) Test specimen in the INSTRON material testing machine

A total of 36 tests have been conducted in the experimental part of this work, three samples for each angle value. All energy absorption indicators calculations have been done in Python. Trapz function from Python NumPy library, which uses the composite trapezoidal rule to calculate an area under a curve, is utilized to calculate the area under the load-displacement curves resulted from the compression tests. The load-displacement curves were split into three parts: the pre-crushing phase, post-crushing phase, and material densification phase, as illustrated in Figure 12. The readings starting from the material densification phase are removed. The resulting data and the calculated indicators will be used to analyze the hexagonal energy absorption devices' crushing behavior and energy absorption performance to train the ANN predictive models.

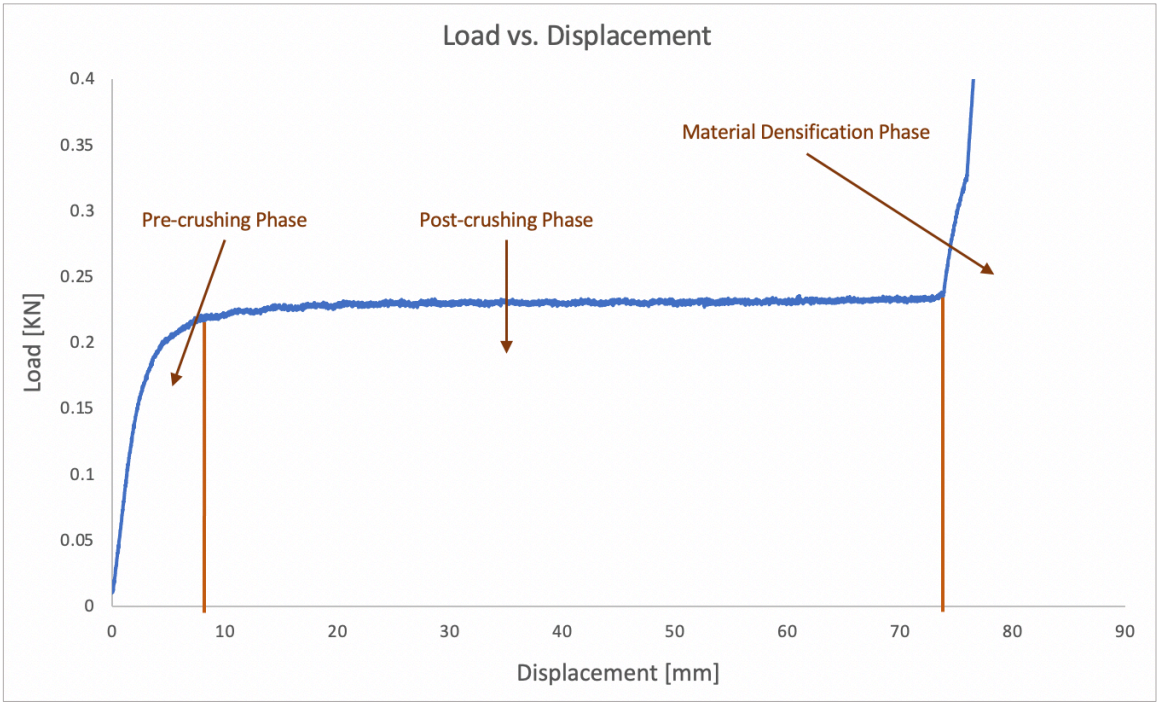

Figure 12. Pre-crushing, post-crushing, and material densification phases of 40° sample

3.2. Experimental work Results and Discussions

3.2.1. Load-Displacement Curves Analysis

In this section, the results of quasi-static axial compression tests carried out on the various hexagon angles are presented, categorized, and discussed. Figure 13 to Figure 24 shows the load-displacement curves resulting from the test and the corresponding images captured from the videos recorded during compressing the specimens with notations that relate the different stages in the plot with the images to identify the crushing behavior of the samples. From the images, it can be seen that all the hexagonal structures with different internal angles are crashing down with the same mechanism.

From these figures, it can be noticed that there are two main behaviors showed in the load-displacement curves. The first one is from 35° to 55° with the corresponding figures from Figure 13 to Figure 17. Taking the hexagon with 35° angle specimen in Figure 14 Figure 6 as an example, notation 2 locating the initial peak force in which after it the specimen keeps on crushing smoothly through notations 3 and 4 while maintaining the IPF almost constant as the displacement increase from about 10 mm to about 70 mm. Notation 5 marks the start of the material densification as seen in the corresponding image 5, the deformed top and bottom of the specimens are in touch, which caused the force to increase as shown in the plot in between notations 5 and 6 until the specimen is completely crushed as shown in the corresponding image 6 in Figure 14.

The second group with similar behavior is shown in the figures from

Figure 19 Figure 24 for the angles from 60° to 85°, respectively. Taking angle 60° in

Figure 19 as an example here, it can be seen that the load reaches its peak at notation 2 relatively faster and at lower displacement. The load then starts to drop through notation three till reaching notation four as the structure is smoothly compressed down and the displacement is increasing. When reaching notation 4, it is shown from the corresponding image four that parts of the deformed structure are touching the machine's upper and lower plates, which required a higher load to compress. Then the load dropped as the compression proceeds till the upper and lower sides of the hexagonal structure start touching, which initiate the material densification phase where the load is increasing while displacement is constant as the specimen is completely crushed.

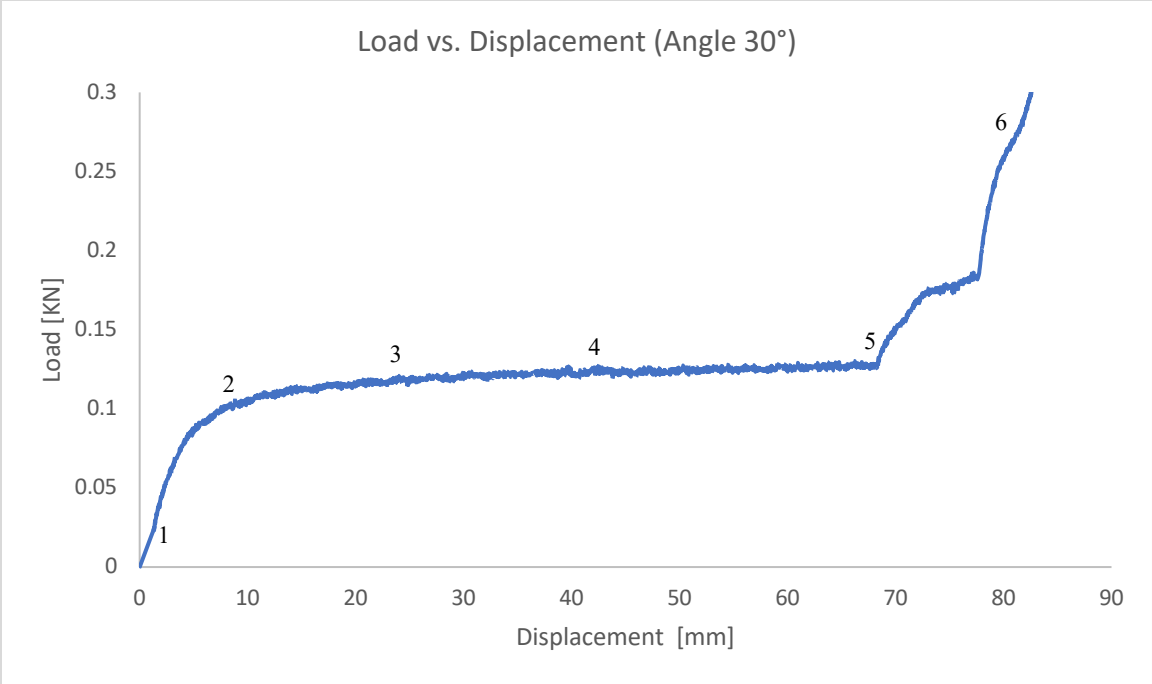

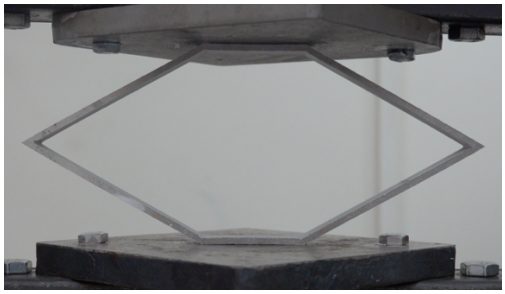

1

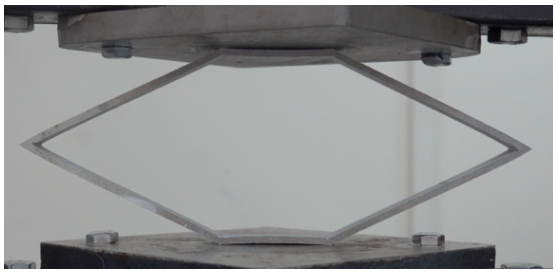

2

3

4

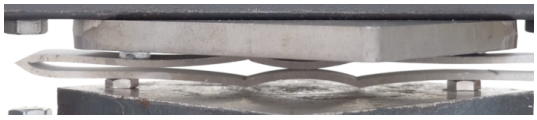

5

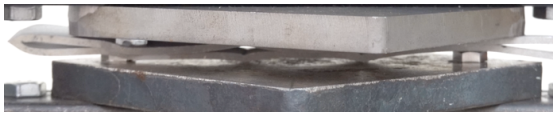

6

Figure 13. Load displacement curve for in-plane compression test of 30° hexagon and corresponding through test images.

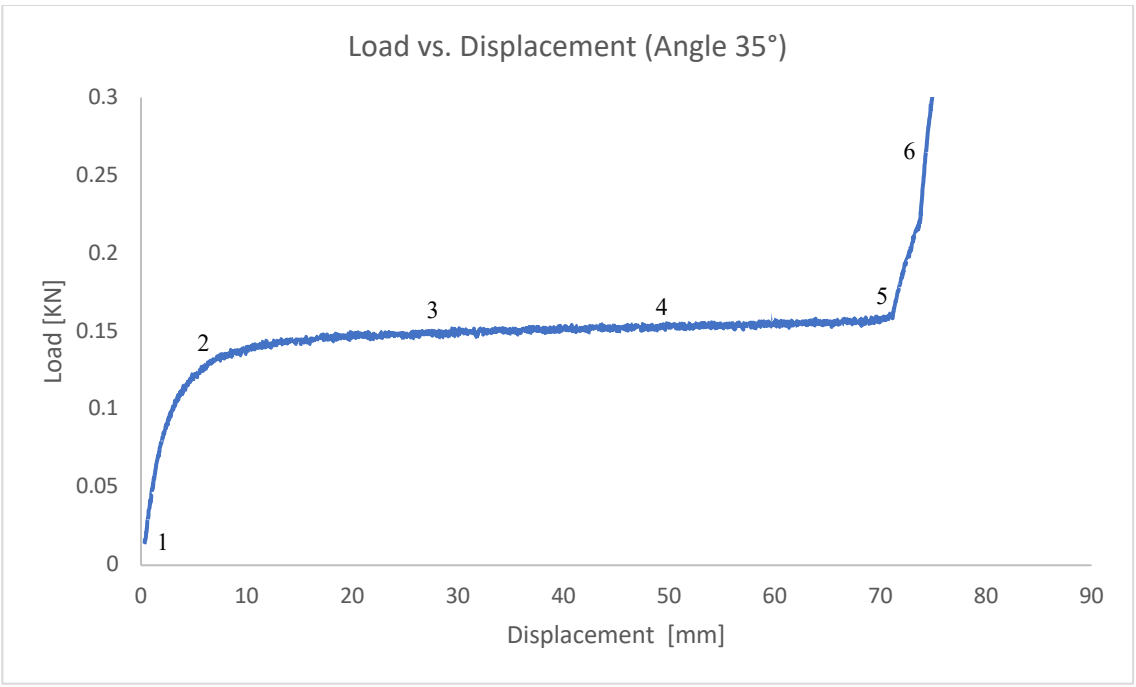

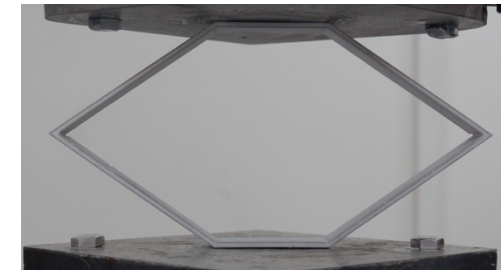

1

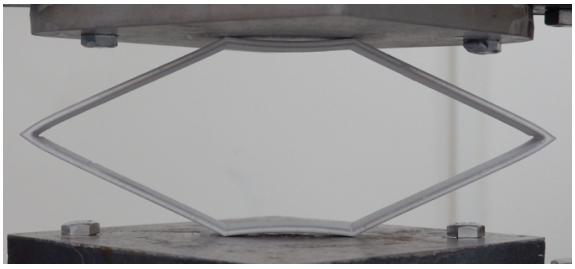

2

3

4

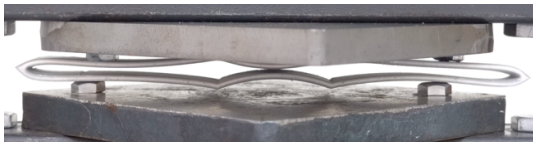

5

6

Figure 14. Load displacement curve for in-plane compression test of 35° hexagon and corresponding through test images.

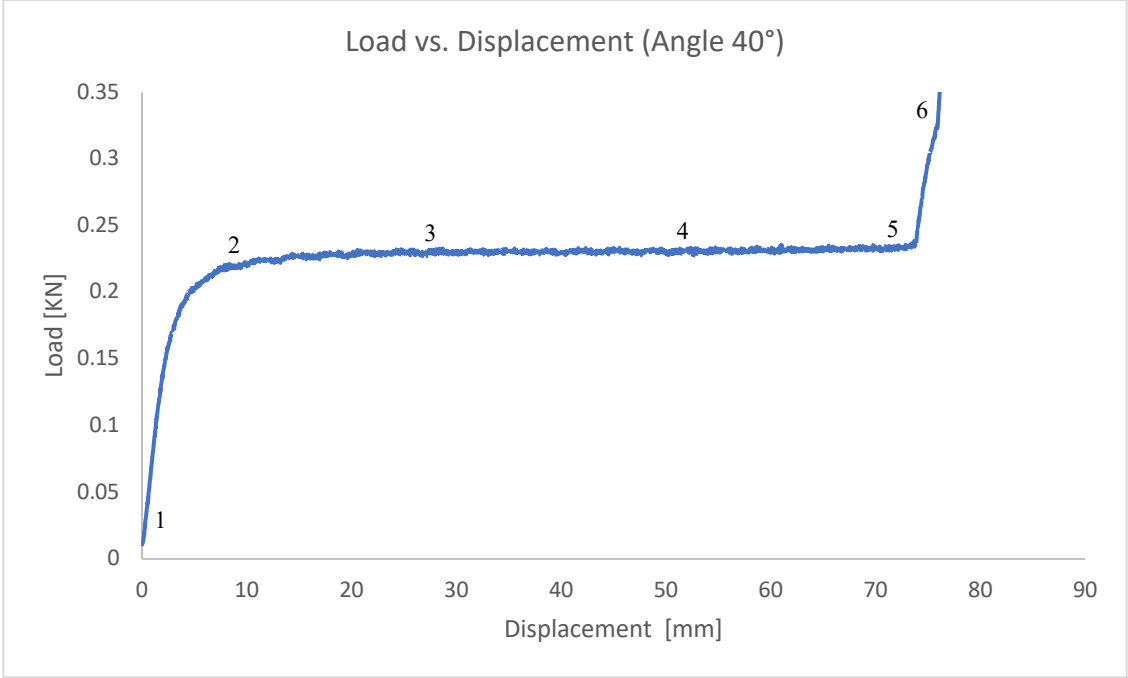

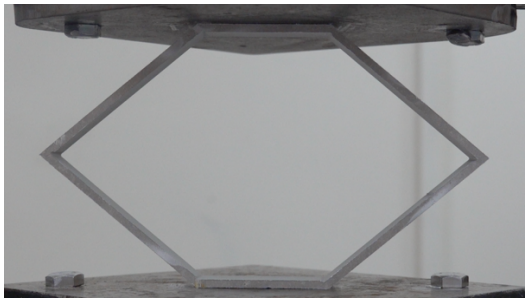

1

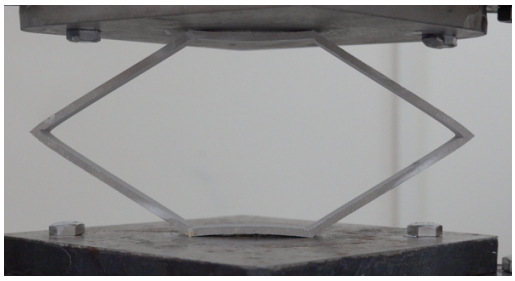

2

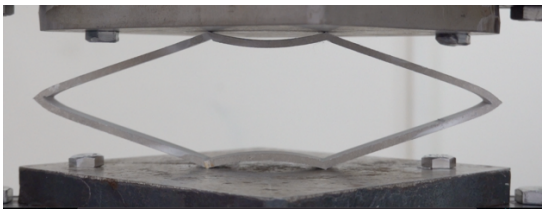

3

4

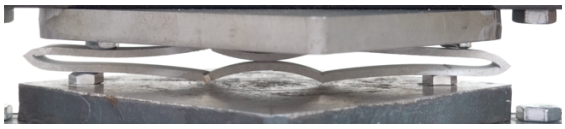

5

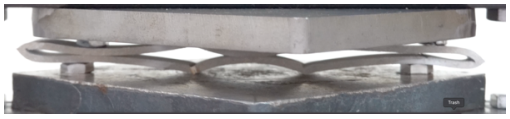

6

Figure 15. Load displacement curve for in-plane compression test of 40° hexagon and corresponding through test images.

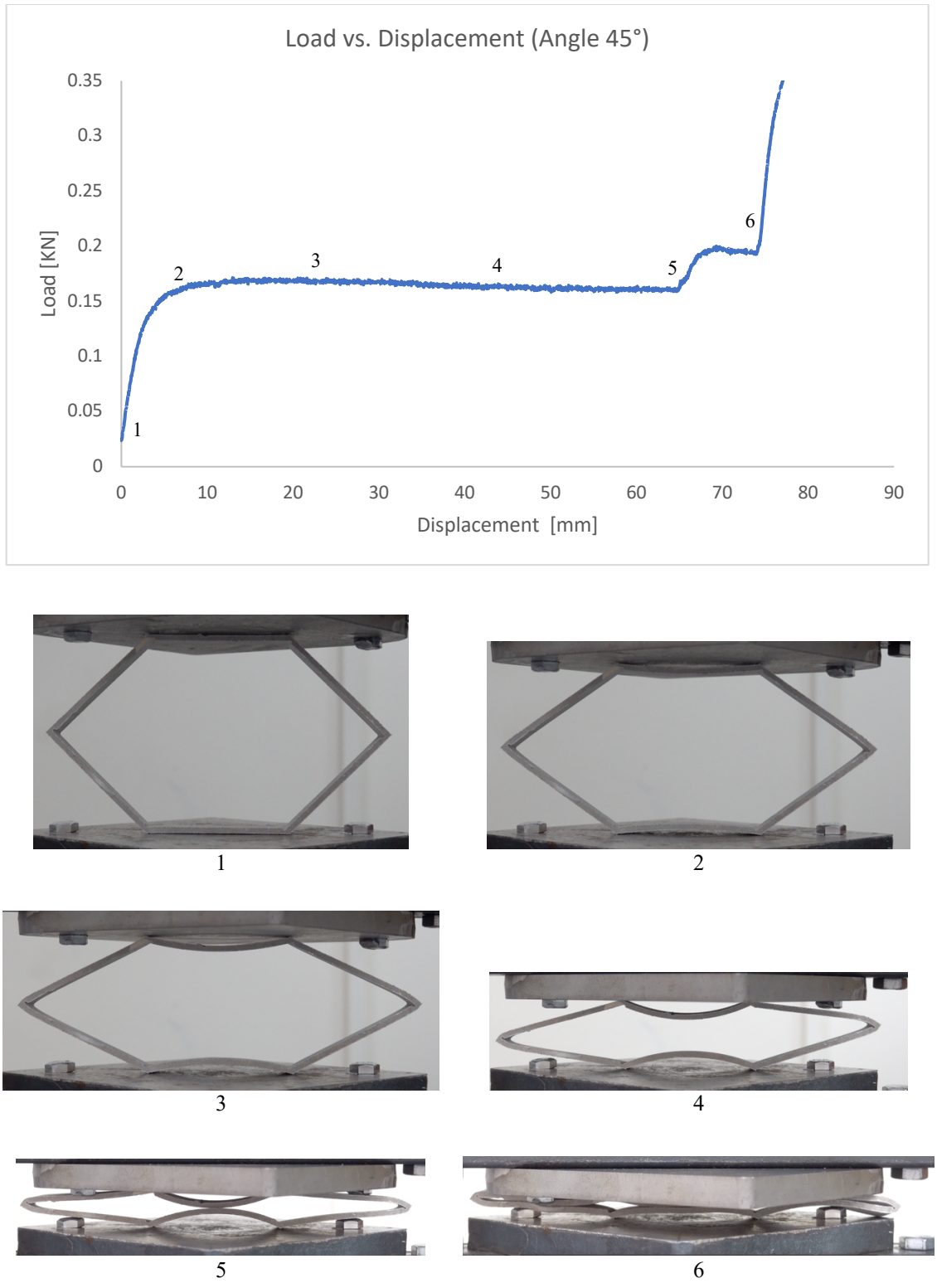

Figure 16. Load displacement curve for in-plane compression test of 45° hexagon and corresponding through test images.

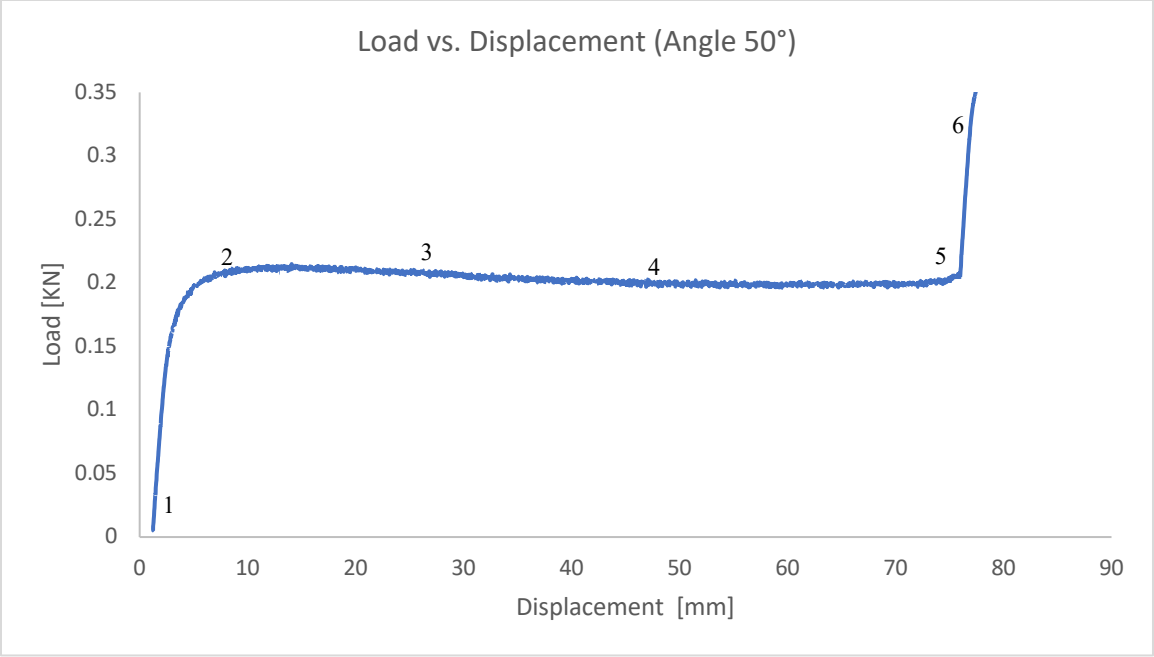

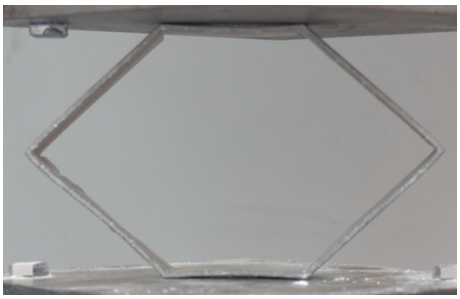

1

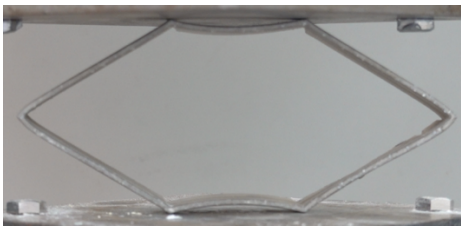

2

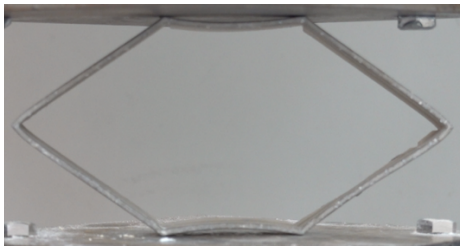

3

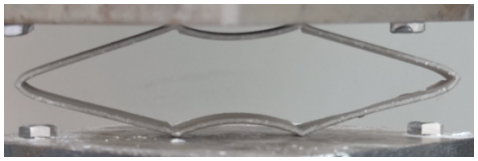

4

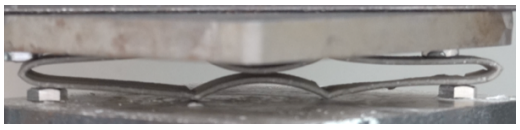

5

6

Figure 17. Load displacement curve for in-plane compression test of 50° hexagon and corresponding through test images

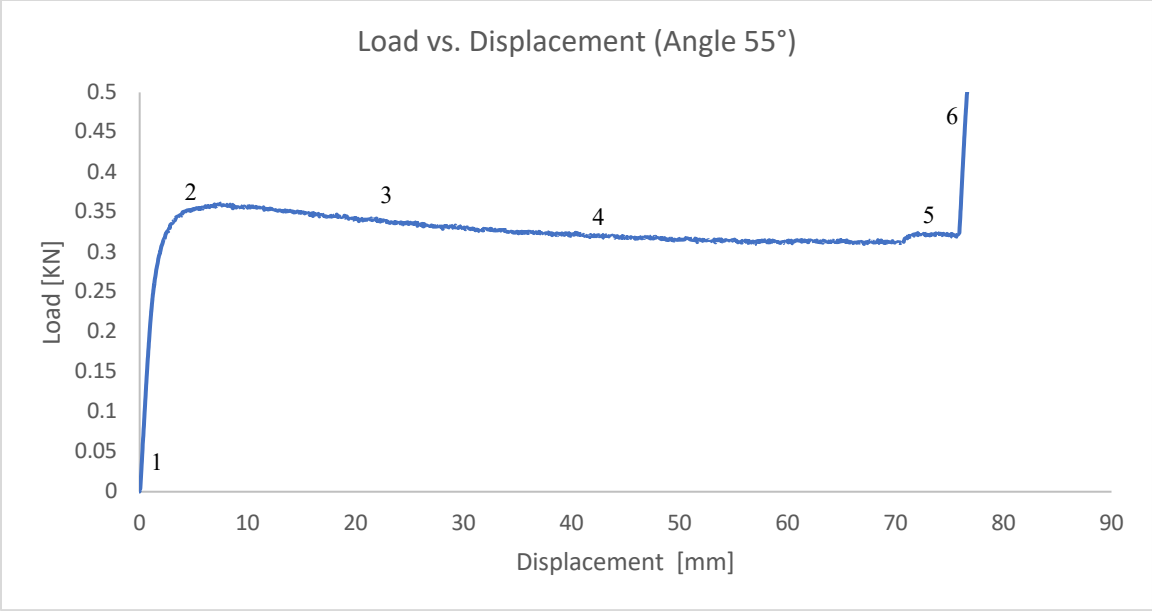

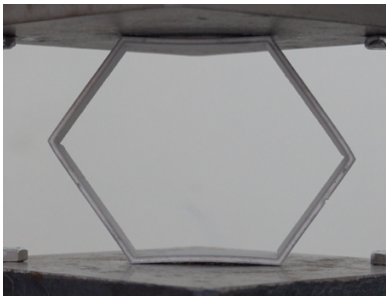

1

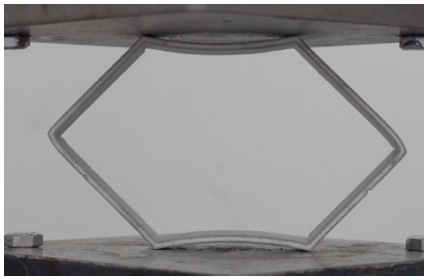

2

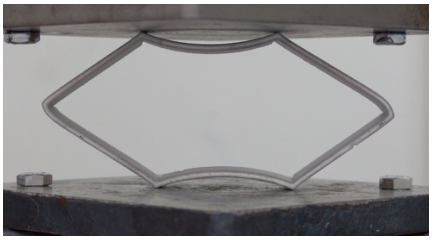

3

4

5

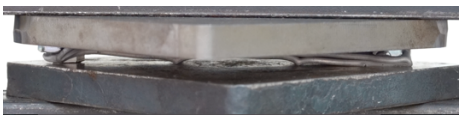

6

Figure 18. Load displacement curve for in-plane compression test of 55° hexagon and corresponding through test images.

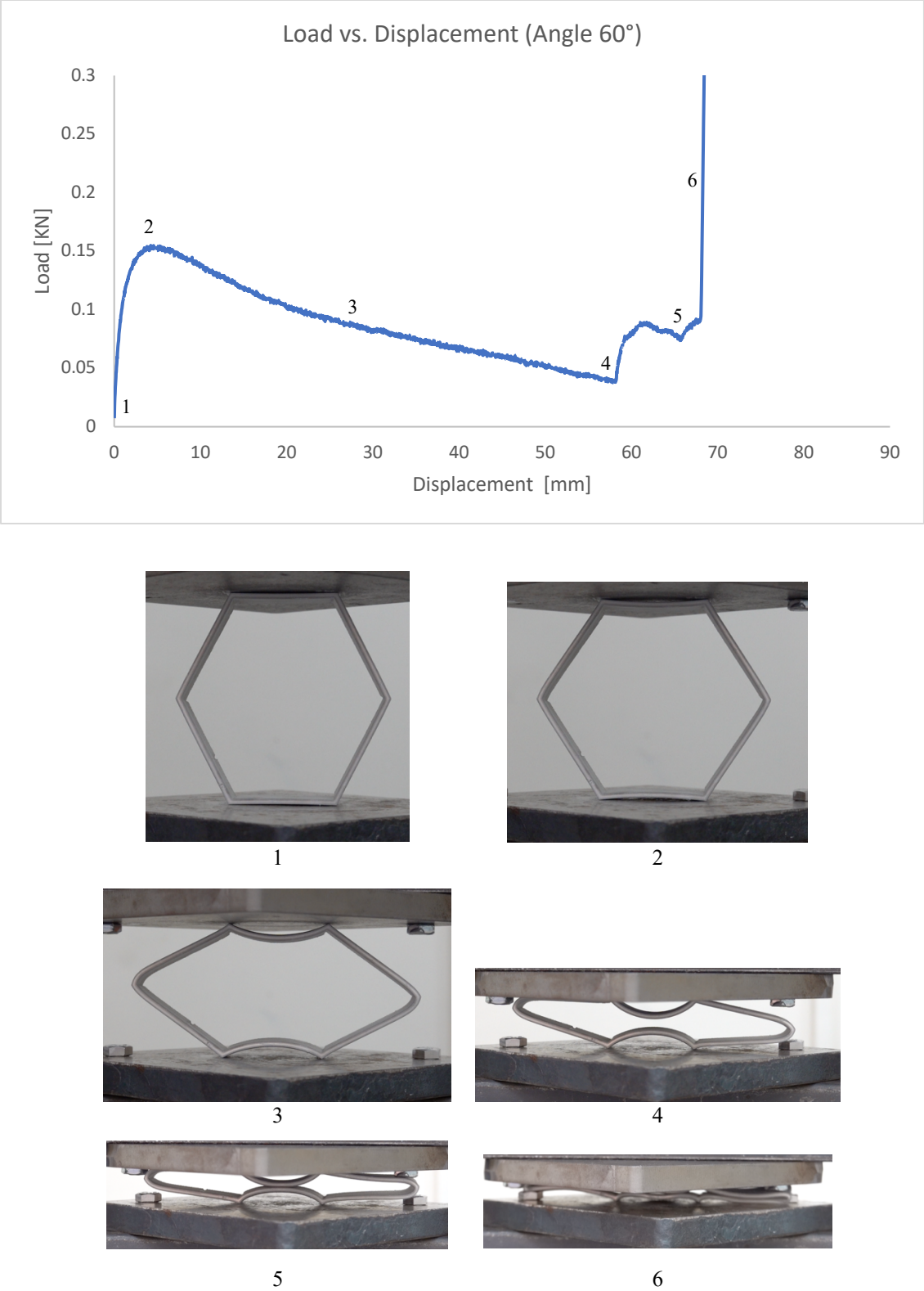

Figure 19. Load displacement curve for in-plane compression test of 60° hexagon and corresponding through test images.

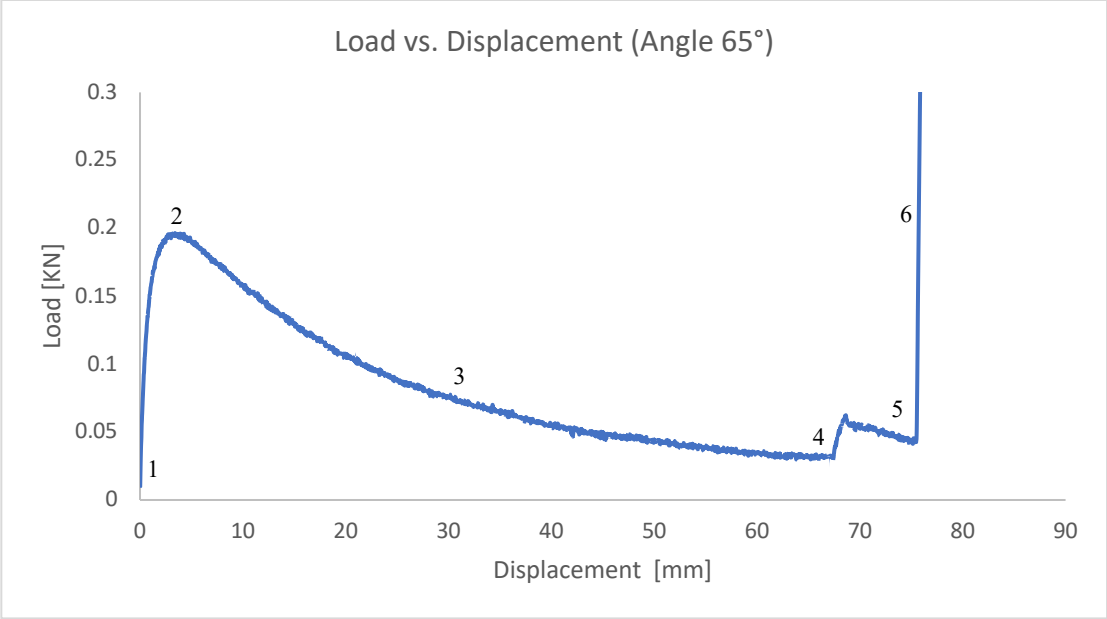

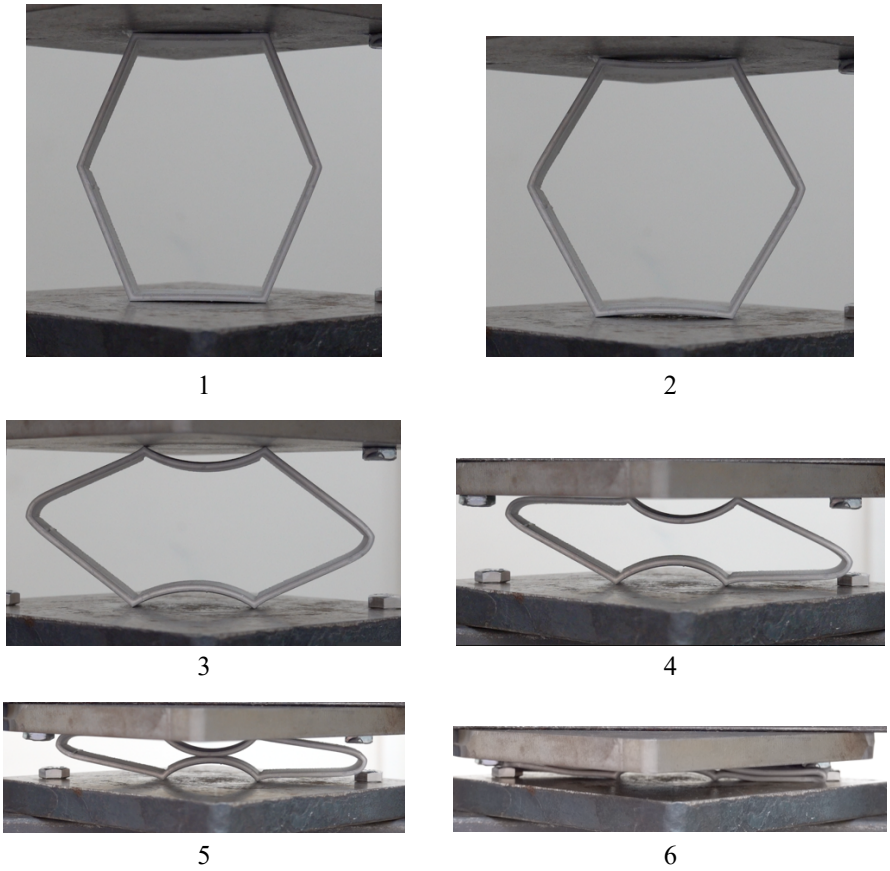

Figure 20. Load displacement curve for in-plane compression test of 65° hexagon and corresponding through test images.

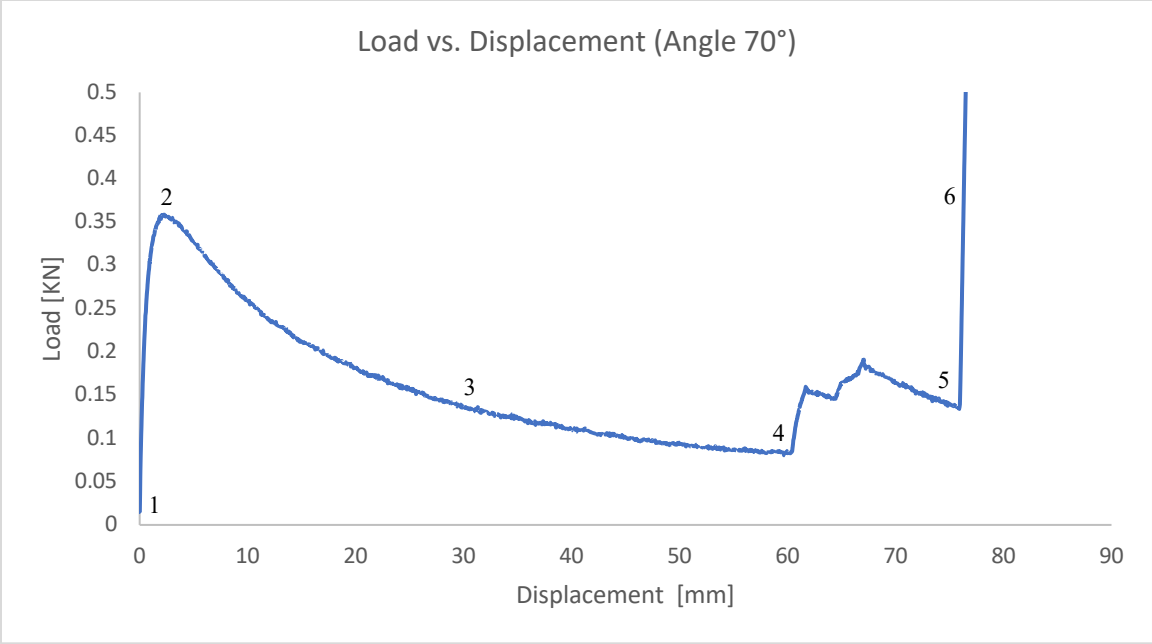

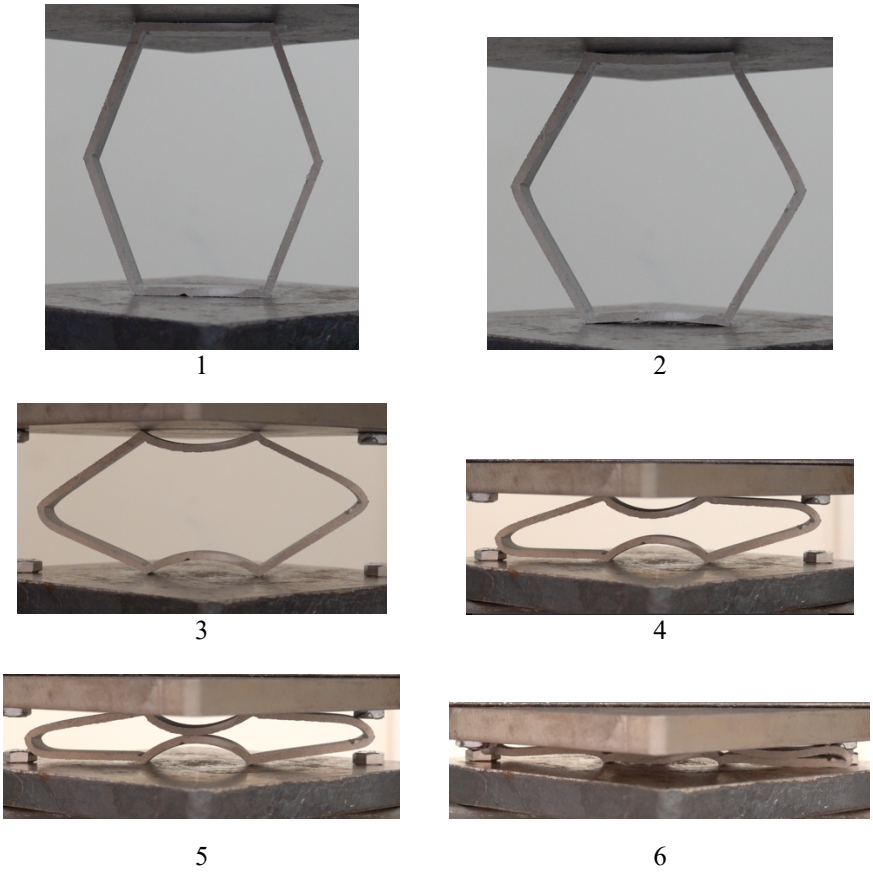

Figure 21. Load displacement curve for in-plane compression test of 70° hexagon and corresponding through test images.

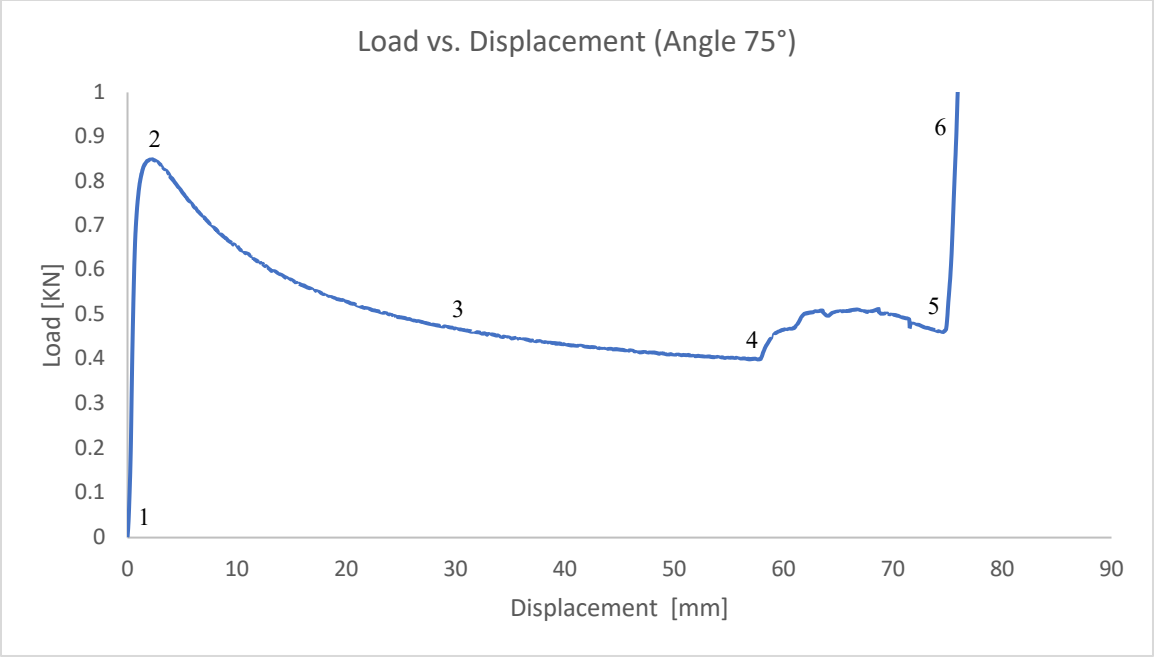

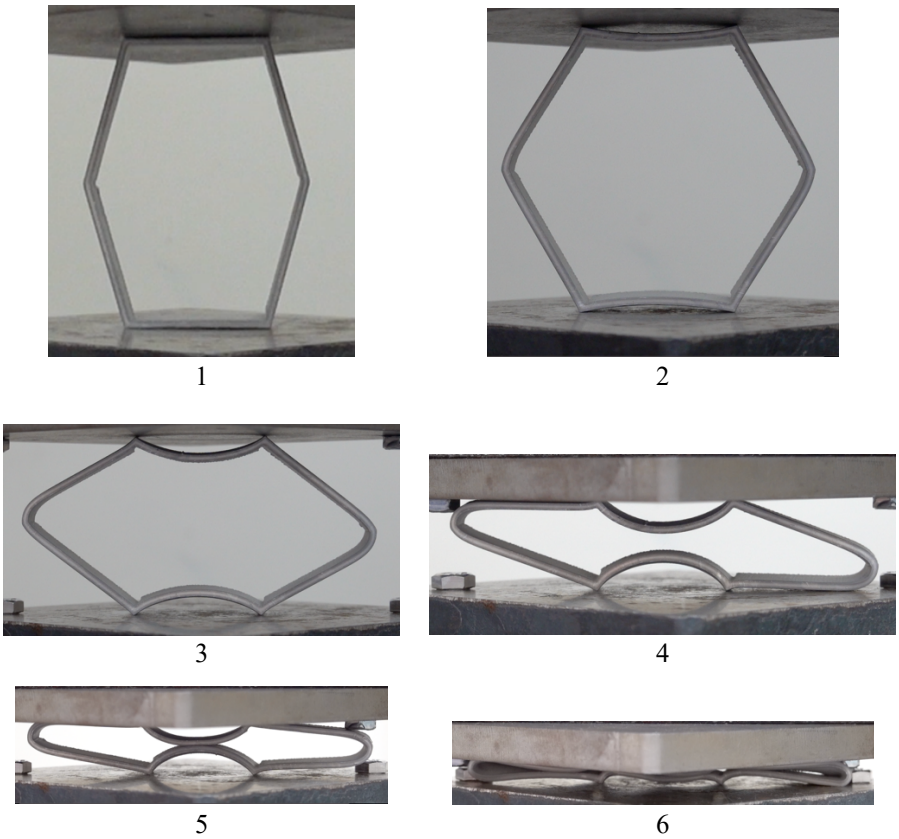

Figure 22. Load displacement curve for in-plane compression test of 75° hexagon and corresponding through test images.

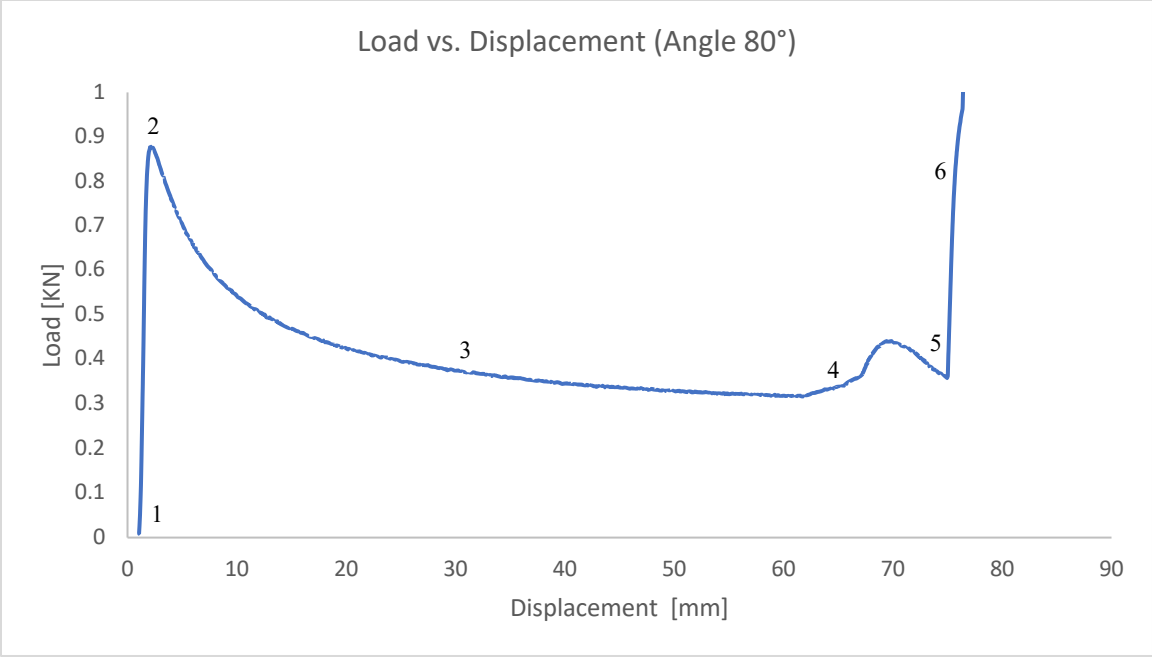

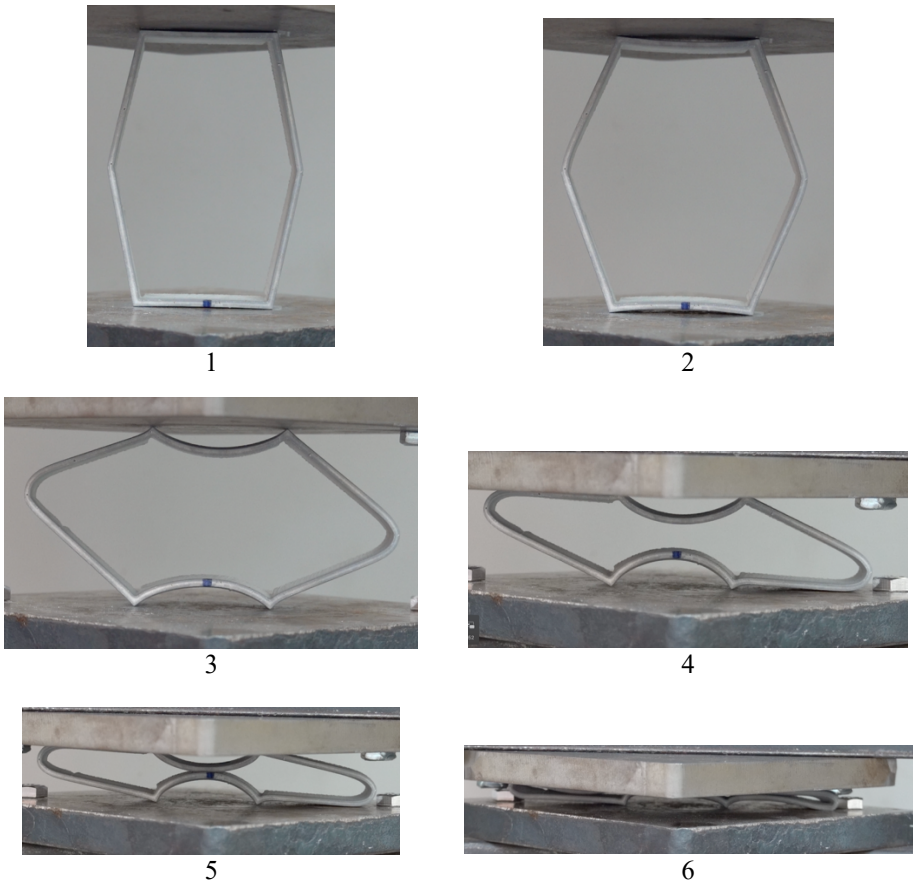

Figure 23. Load displacement curve for in-plane compression test of 80° hexagon and corresponding through test images.

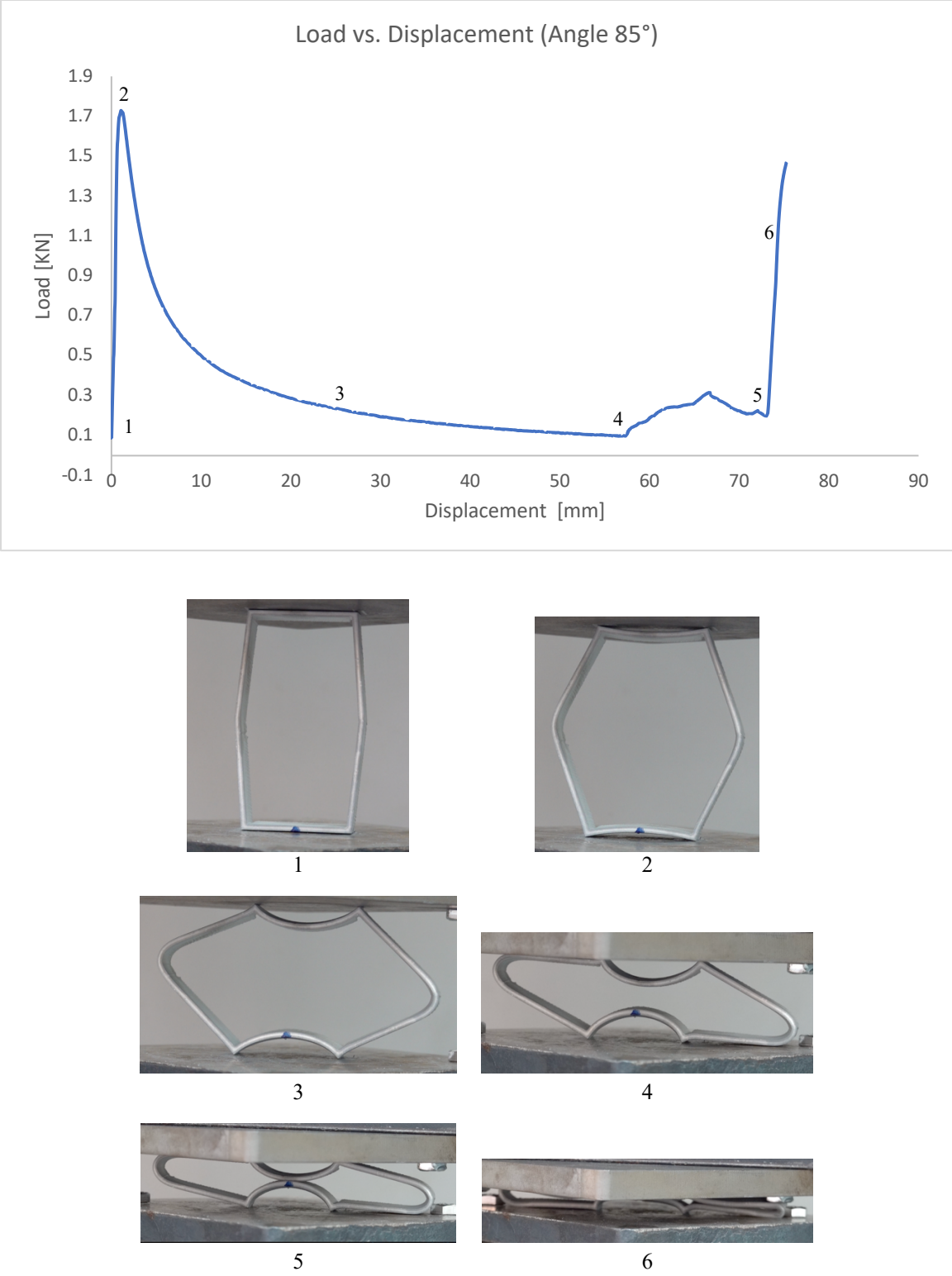

Figure 24. Load displacement curve for in-plane compression test of 85° hexagon and corresponding through test images.

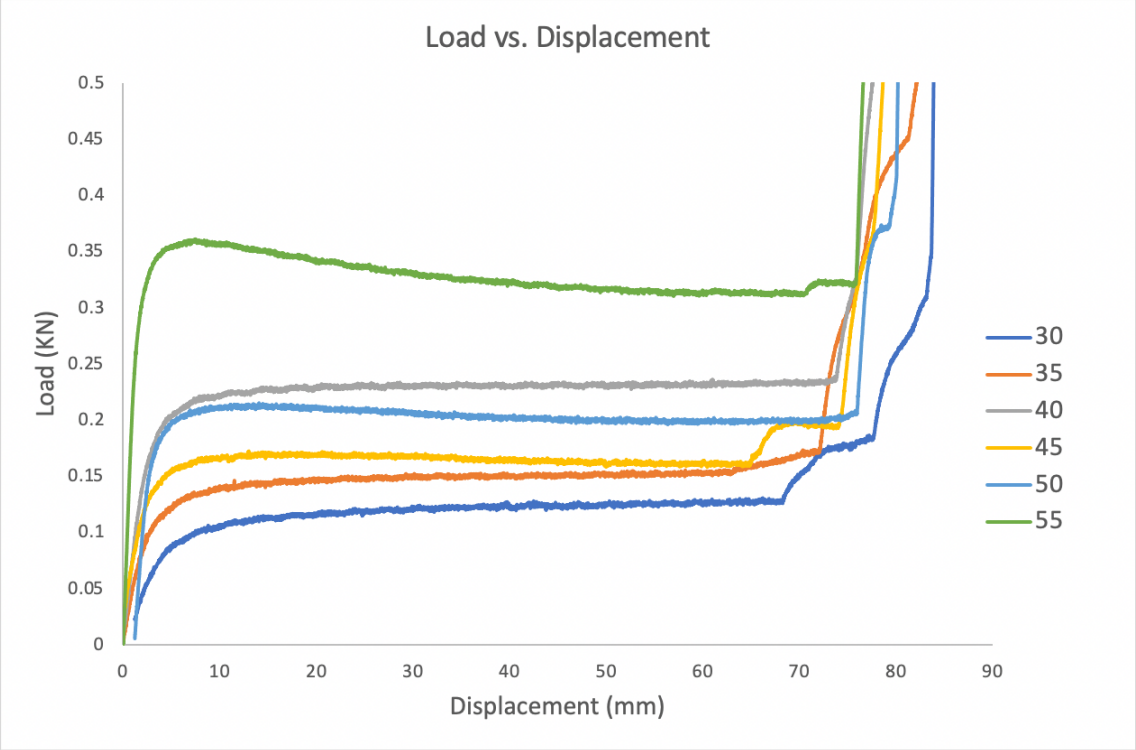

Figure 25. Load displacement curves for in-plane compression test of the hexagons with angles from 30° to 55°.

Based on the crushing behavior of the samples, they can be grouped into two categories. The first one in Figure 25 shows the angles from 30° to 55° having relatively similar behavior under the axial compressive load where the initial peak load is very close to the mean crushing force compared to the other group of angles in Figure 26. The maximum IPF is 0.1KN at 9.9 mm displacement, which marks the end of the specimen's elastic deformation stage. The compressive load remained almost at a constant value during the post-crushing phase while the displacement is increasing as the samples are being compressed; this indicated that these specimens have a very high crushing force efficiency. In other words, that the specimens did not experience a noticeable drop in load-bearing

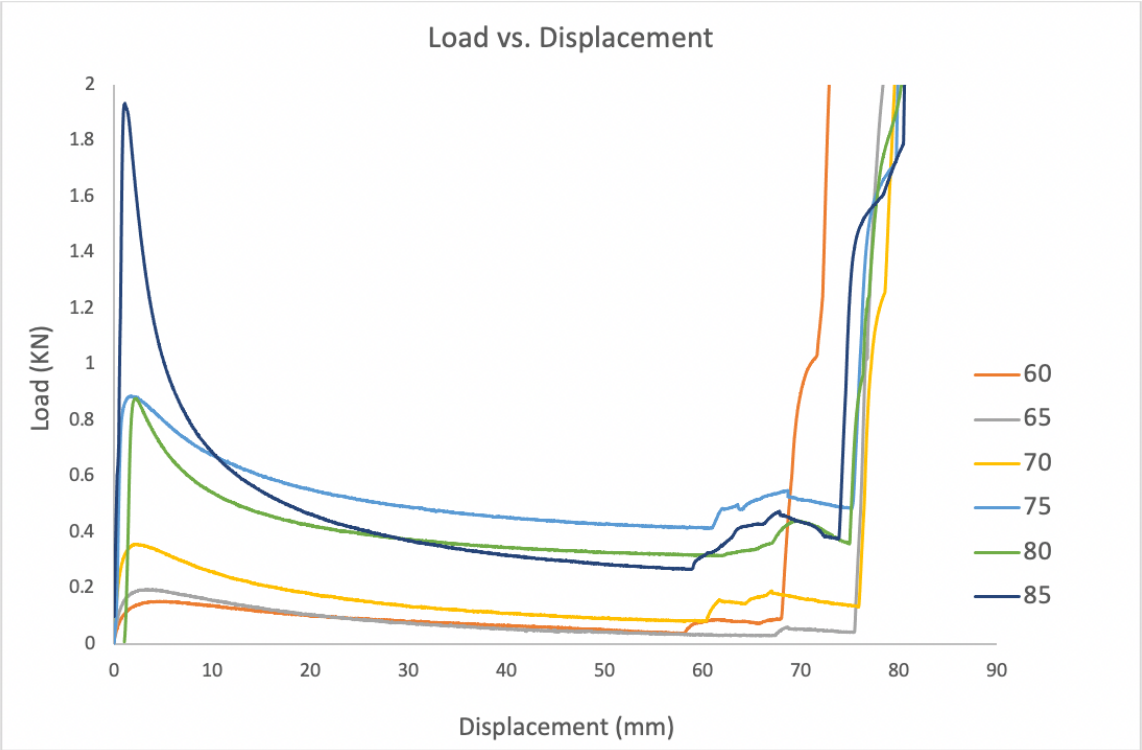

Figure 26. Load displacement curves for in-plane compression test of the hexagons with angles from 60° to 85°

capacity after reaching the initial peak force as it continues to bear the load while crushing down. The constant load values in the plots shown in Figure 25 continue until reaching the material densification phase, where the upper and lower sides of the specimens are in contact, and the specimens are completely crushed flat, which causes the load to spike up.

The load-displacement curves in Figure 26 show the rest of the angles, from 60° to 85°. Hexagonal rings with the angles: 60°, 65°, and 70° showed similar behavior to the angles in Figure 25 but with a slight drop in the load-bearing capacity after reaching the initial peak force. The load starts to decrease slowly as the displacement increase during the post-crushing phase until it spikes up when reaching the material densification phase.

For hexagons with the larger angles of 75°, 80°, and 85°, the pre-crushing phase is much smaller than it is in the smaller angles. The load reached the initial peak force faster at small displacements of between 0.7 and 3 mm. After this peak, the load drops suddenly during the post-crushing phase. Due to the sudden drop in the load, the specimens would have a low crushing force efficiency, which means a less crushing mechanism.

One of the main differences between the load-displacement plots in Figure 25 and Figure 26 is the small increase in the load shown in Figure 26 before entering the material densification phase. The reason behind it can be observed through the test images in the figures from

Figure 18 to Figure 24, where the specimens are tilted to one side as they are being compressed down. When the specimen is tilted, the deformed sides became in contact with the machine's upper and lower plates, which caused the load to increase to continue compressing the specimen until entering the material densification and making the specimen completely flat. This behavior could be due to imperfections existing from the fabrication process or other reasons.

3.2.2. Energy Absorption Performance Indicators

All of the calculations for the energy absorption indicators have been done in Python Jupiter Notebook as it provides an efficient computing environment for data calculations and analysis. Table 1 contains all of the calculated values of the energy absorption indicators: specific absorbed energy, the pre-crushing absorbed energy, the post-crushing absorbed energy, the initial peak force, the mean crushing force, and the crushing force efficiency. While

Table 2 shows the angles with the highest and lowest values of the energy absorption indicators. Starting from the specific energy absorption, from the values in Table 1, it can be seen that the change in SAE as the angle values increase is not linear. The lowest specific energy was absorbed by angle 30°, while the highest was achieved by angle 75°. The specific energy was absorbed in the pre-crushing phase was also non-linear as the angle values increased linearly; the highest was achieved by angle 50° while the lowest values achieved by the angles 30° and 65°. Thus, the highest SAE in the elastic deformation region of the hexagonal structures was by angle 50°. For the post-crushing phase, where the major amount of the energy is absorbed, the most considerable amount of energy per unit mass was absorbed was by the hexagon with an angle of 75° followed with angle 80°, and the hexagon absorbed the lowest energy per unit mass with an angle of 30°.

The initial peak force is one of the most important indicators when evaluating the energy absorption performance as it marks the force required to take the test specimen from the elastic to the plastic deformation region. Here, the highest IPF reported was for angle 85° at a value of 1.86 KN, followed by angle 80° at a value of 0.80 KN. The lowest IPF values were for angles 30° at 0.1 KN. Angles with low IPF means they showed less resistance to the deformation caused by the compressive force due to their low load-carrying capacity.

The mean crushing force is the mean force the structure experience during the post-crushing phase. It is essential to evaluate the crushing force efficiency of each structure. The closer the MF to the IPF, the more stable the crushing behavior is. The CFE, as stated before, is the ratio of the MF to the IPF. The ideal CFE is one, as this indicates that the IPF is sustained throughout the post-crushing phase, which means the failure mechanism is

stable through this phase. The best CFE was achieved by angle 45° at 97.1%. The first three angles (30°, 35°, and 40°) have CFE greater than one (1.174, 1.080, and 1.030, respectively) it means that the MF is greater than the IPF, it can be seen in Figure 25 that the plots of these angles are slightly increasing during the post-crushing phase. However, the CFE values are very close to one for these angles. From Table 1, it can be seen that the CFE starts decreasing from angle 60° where it decreased from 95.3% for angle 55° to 69.2% for angle 60°. CFE decreased even more for angle 65° to reach 33.9% then it increased to be around 50% for angles 70°, 75°, and 80°. Lastly, the CFE decreased to reach 21.9% for the hexagon with the largest angle.

From these results, it can be noticed that there is not only one optimal angle that has the best performance based on all of the calculated indicators in Table 1. The optimal angle will be different based on the application it will be used for. For example, suppose the hexagonal structure will be used as an energy absorption device in a vehicle where the crushing stability is very important. In that case, the hexagon with an angle of 45° can serve this application best for its low IPF and high CFE. Energy absorbers in automobiles are preferred to have a lower initial peak crushing force and stable failure to minimize injuries the vehicle passengers could be exposed to during collision accidents and minimize damage to the vehicle's critical components. On the other hand, if the application requires the structure to have the best load carrying capacity and to resist any compressive loads, a hexagonal structure with 85° interior angles should be used as it requires 1.86KN (highest IPF) for the structure to start crushing and deforming plastically.

In the following chapter, the data extracted for the tests will be used to train and test ANN models in order to optimize the hexagonal energy absorber design based on any specific application and targeted properties.

Table 1. Quantitative Energy Absorption Performance Indicators.

S/N	Angle	Specific Absorbed Energy [J/Kg]	Pre-crushing Specific Absorbed Energy [J/Kg]	Post-crushing Specific Absorbed Energy [J/Kg]	Initial Peak Force [KN]	Mean Crushing Force [KN]	Crushing Force Efficiency [KN/KN]
1	30	93.33	7.62	85.71	0.10	0.11	1.17
2	35	140.97	13.59	127.38	0.14	0.15	1.08
3	40	255.02	25.92	229.10	0.22	0.23	1.03
4	45	194.21	34.44	159.77	0.17	0.16	0.97
5	50	289.28	48.12	241.16	0.20	0.19	0.95
6	55	514.35	40.71	473.64	0.39	0.38	0.95
7	60	210.32	18.04	192.29	0.23	0.16	0.69
8	65	99.61	10.16	89.46	0.18	0.06	0.34
9	70	360.49	18.03	342.46	0.42	0.23	0.53
10	75	795.55	27.23	768.31	0.85	0.51	0.60
11	80	728.70	18.79	709.91	0.80	0.40	0.49
12	85	657.33	24.32	633.01	1.86	0.41	0.22

Table 2. Hexagon's Angles Ranking Based on Energy Absorption Performance

Specific absorbed energy [J/Kg]		Pre-crushing specific absorbed energy [J/Kg]		Post-crushing specific absorbed energy [J/Kg]		Initial peak force [KN]		Mean crushing force [KN]		Crushing force efficiency [KN/KN]	
Highest	Lowest	Highest	Lowest	Highest	Lowest	Highest	Lowest	Highest	Lowest	Highest	Lowest
75°	30°	50°	30°	75°	30°	85°	30°	75°	65°	40° & 45°	85°

CHAPTER 4. ARTIFICIAL NEURAL NETWORK

This chapter presents the predictive study by artificial neural network developed for this work. The first section is the methodology used, where it starts with data preprocessing, then neural networks models development, followed by presenting the steps of building, training, and validating the models. The second section presents and discusses the models' results and applying the predictive model to optimize the hexagonal energy absorber for different applications.

4.1.Methodology

4.2.Data Preprocessing

Data preprocessing is the technique of preparing the raw data to make it suitable for building and training a machine learning model. In this case, it is an ANN model. It is an important step to enhance the quality of data and facilitate the extraction of useful insights from the data. The first step in data preprocessing is to make sure that the data are in a suitable format and free from missing data, outliers, and erroneous data values. The next step is feature extraction. It is necessary to identify the independent variables to be the model input and the dependent variable to be the output. In this case, six features were identified, which are the energy absorption performance indicators (e.g., initial peak force, specific absorbed energy, specific absorbed energy of the pre-crushing phase, specific absorbed energy of the post-crushing phase, mean crushing force, and crush force efficiency) in addition to the angle which is the variable that will be predicted based on these six features. There will be six input nodes in the input layer and one output node in the output layer in the predictive model. The last step is splitting the data set into a training,

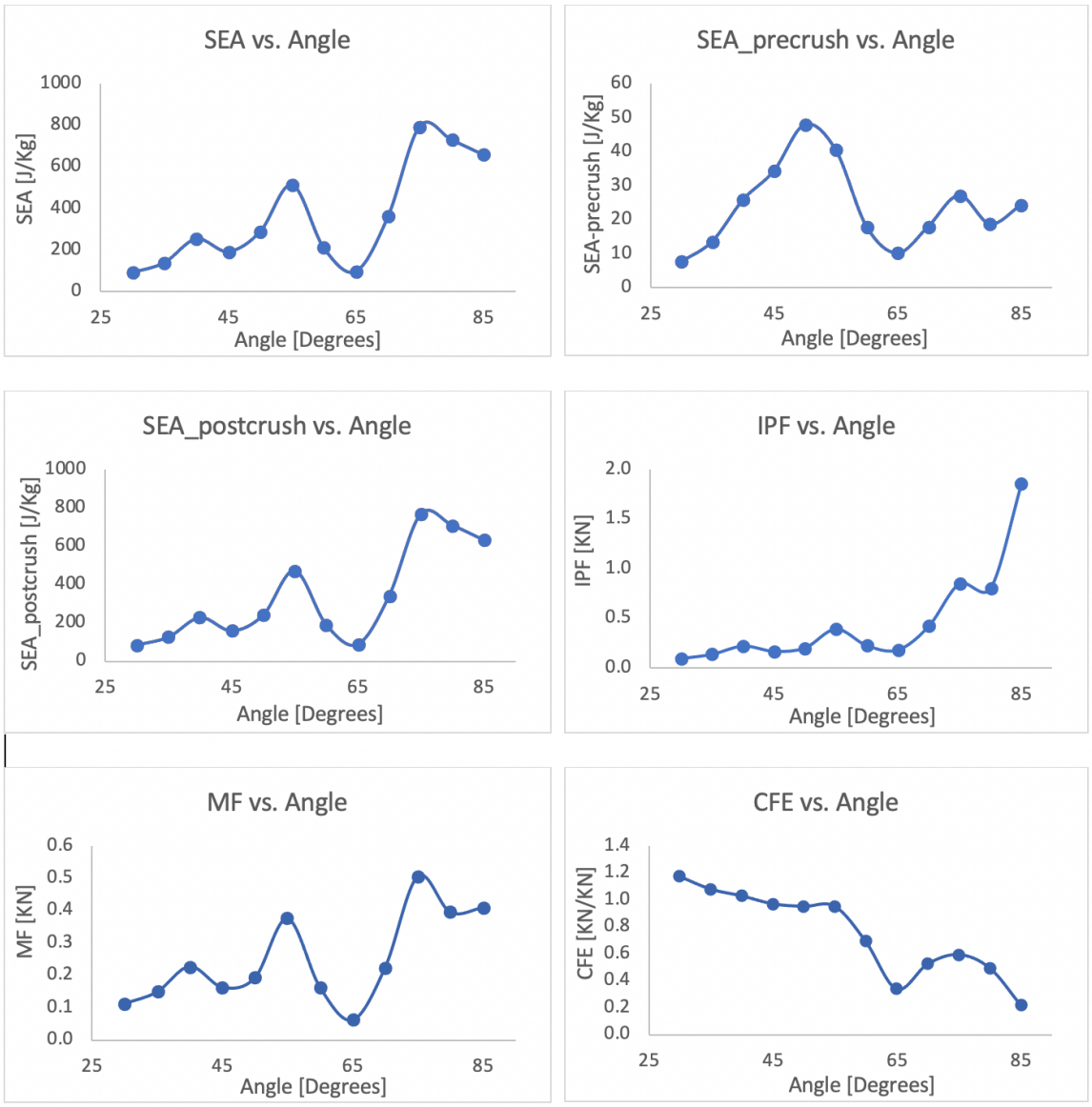

Figure 27. Plots of the independent variable against the dependent variable.

test and validation datasets. The validation dataset was removed manually from the dataset. Since the data is limited, the K-fold cross-validation is used in the training phase as this will allow the whole data set (after removing the validation set) to be used for training and testing simultaneously. Three test specimens were tested for each of the 12 angles shown in Table 1; a total of 36 data points were used to train, test, and validate the

ANN model. Table 1 shows the averaged results of AE performance parameters of each angle, and these parameters have been plotted versus the angles to get an insight into the relationship between them and identify which regression model is best suited for predicting the optimal angle. From Figure 27, it can be seen from the plots that all of the features have a non-linear relationship with the variable to be predicted. Thus, the artificial neural network machine learning algorithms might be the best suited for solving its problem due to their high capability to learn the non-linear relationship between the data.

4.1.1. Model Development

The main challenge for the regression is the limited data points, thus developing a model that can efficiently learn from the available data, which are the energy absorption indicators, will not be straightforward. Due to the data's nonlinearity, a classical optimization/regression model cannot give good predictions. Hence, the ANN model can learn complex non-linear relationships between the data through its hidden layers that consist of neurons that a suitable learning algorithm can train. One of the standard methods of training artificial neural networks is the backpropagation algorithm. It is a learning method for multilayer feedforward networks that calculates the gradient of a loss function for all the weights in the network, then modifying the input variables' internal weightings to produce an expected output variable. The error between the model's output and a known actual output is presented to the model and used to modify its internal parameters.

The key to building the ANN predictive model is to find the right architecture. The ANN architecture is the structure of the model; it consists of parameters such as the number of hidden layers, epoch, batch size, etc. Other parameters are learned automatically by the

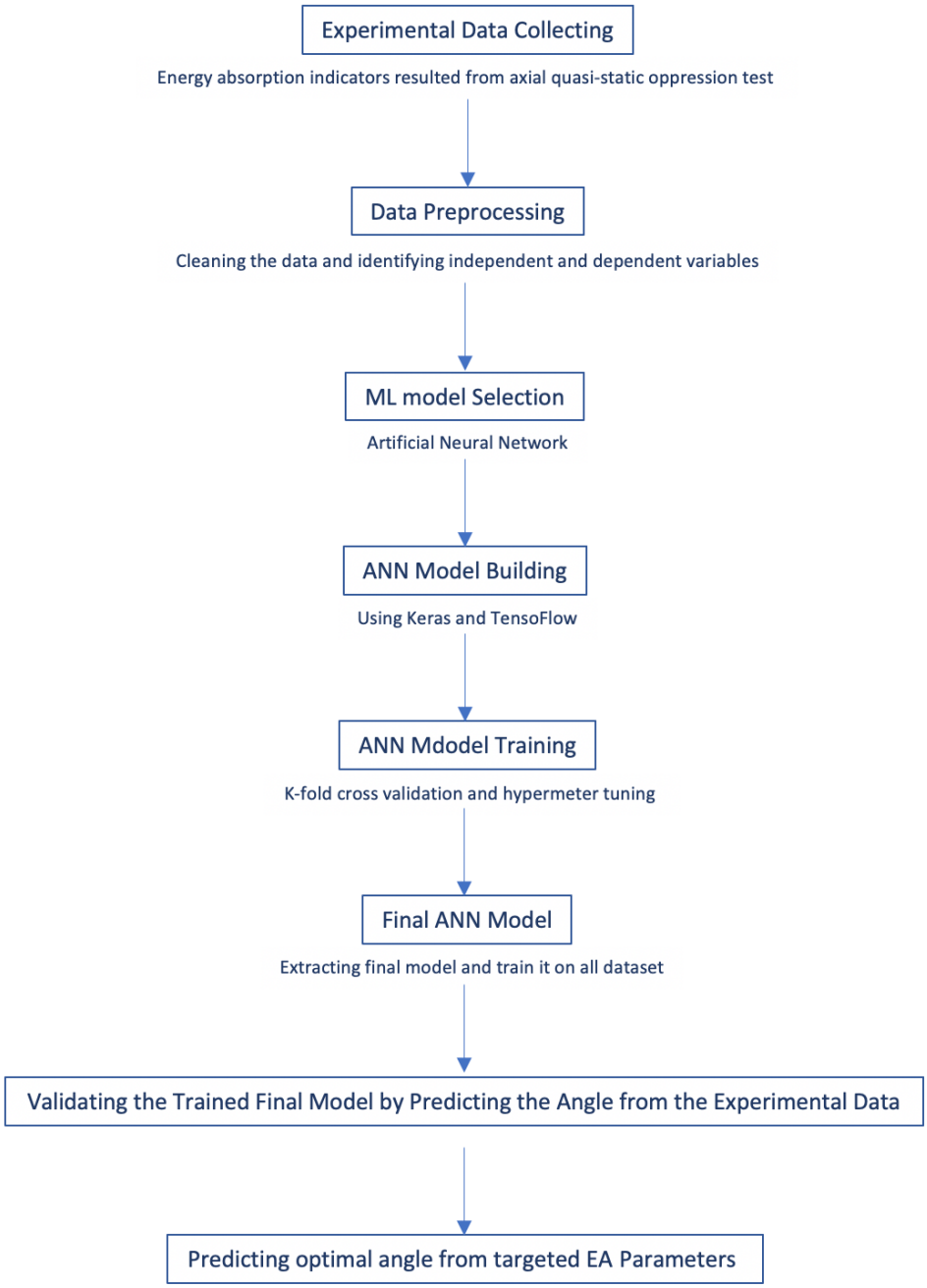

Figure 28. Strategic steps for ANN model development and prediction

algorithm, such as node weights, bias, etc. Moreover, hyperparameter controls the learning process by tuning these hyperparameters to enable the model to solve the machine learning optimally. Problem and reach the desired output. The hyperparameter can be tuned

manually or automatically by using a tuning method, such as a TensorFlow grid search. The flow chart in Figure 28 shows the strategic steps to develop the ANN model.

4.1.2. Building and training the ANN prediction model

The main three steps to build any machine learning model are data preprocessing, model building and training, and model validation through testing and evaluating the trained model performance with a testing data set. The ANN model consists of three layers, which are input, hidden, and output layers. Figure 29 illustrates the structure of the ANN model. The input layer is the beginning of the ANN workflow; it is composed of artificial input neurons that bring the initial input data to the system to be processed by the subsequent layers. The hidden layers are located between the input and output layers; they can be one or more layers. Each consists of many neural elements, which work as mathematical functions designed to produce an output specific to the desired result. The hidden layers perform non-linear transformations of the inputs entered into the network by applying weights and direct them through an activation function.

The ANN model is built using the Keras-Dense layer of the TensorFlow open-source library. The Dense implements the operation [81]:

$$\mathrm{y} = \vartheta\left(\sum wx\right) + b \tag{5}$$

$$\mathrm{output} = \mathrm{activation}(\mathrm{dot}(\mathrm{input}, \mathrm{kernel}) + \mathrm{bias})$$

Where input is the input data, activation is the element-wise activation function passed as the activation argument, and the kernel is a weights matrix created by the layer,

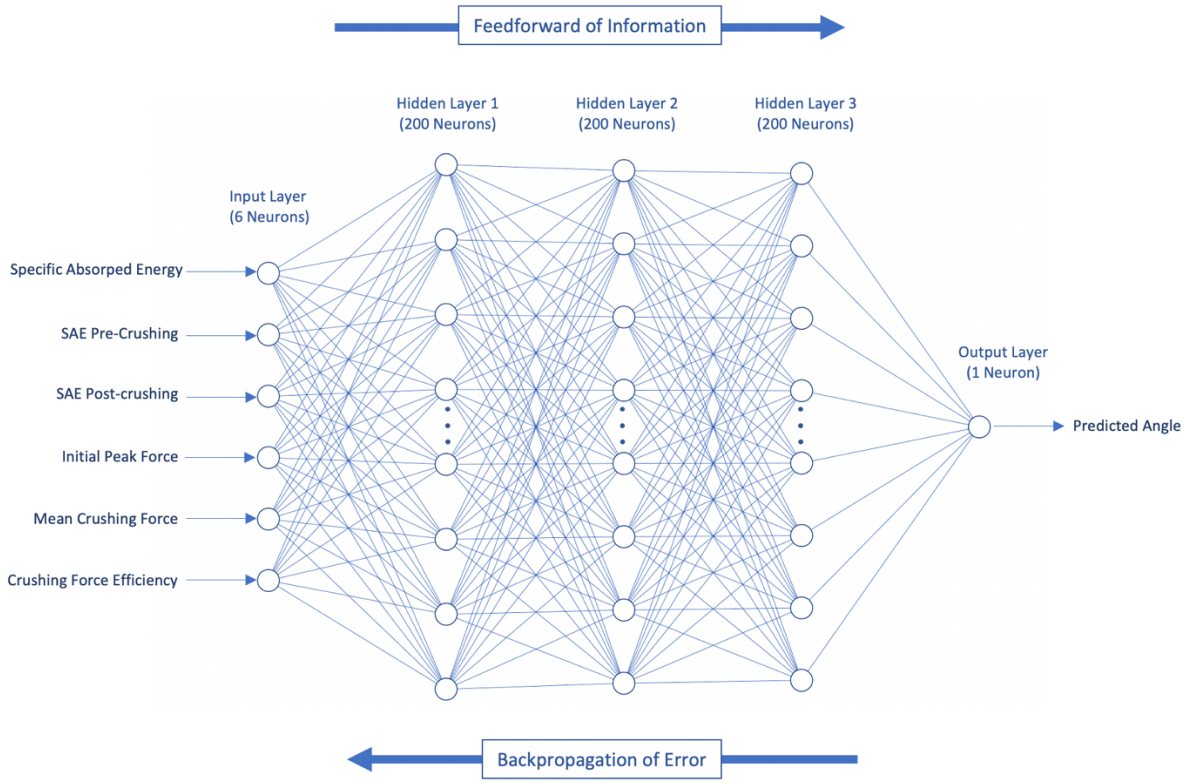

Figure 29. The layered structure of the ANN predictive model

the dot is the NumPy dot product inputs and their corresponding weights, and bias is a bias vector also created by the layer [81]. Rectified linear unit activation function (ReLU) is used as it is one of the most widely used activation functions estimators that can activate all neurons simultaneously and proved that it could greatly improve the performance of feedforward networks [18]. During training the model, several activation functions of Tensor Flow were tested, such as 'sigmoid' and 'Softmax.' However, The ReLU activation function showed better performance, and it is described as follows:

$$f(x) = 0; for\ x < 0 \quad (6)$$

$$f(x) = x; for\ x \geq 0 \quad (7)$$

Adam optimizer is from TensorFlow is used here, as it one of the most used optimizers as it implements the Adam optimization algorithm, which is a stochastic gradient descent method that can calculate individual adaptive learning rates for different variables. The Mean Squared Error (MSE) is used as the loss function in this model. The best iteration and regression were considered based on the lowest MSE value. The MSE equation is as follows:

$$MSE = \frac{1}{N}\sum_{i=1}^{N}(y - \hat{y})^2 \quad (8)$$

Where y is the measured output and $\hat{y}$ is the predicted output. The error is reduced by modifying the weights according to the following equation:

$$\Delta w = -\eta \frac{\partial MSE}{\partial w} \quad (9)$$

Where η is the learning rate, the optimum ANN structure was obtained by the manual and automatic hyperparameter tuning method. The Dropout method was used to prevent the Neural Networks from overfitting. One of the most critical parameters in the configuring ANN model is the number of epochs. Epoch refers to one cycle through the entire training dataset. Too few epochs can lead to under fitted model, while too many epochs can lead to overfitted model. Thus, it is critical to monitor the model performance and indicate the stopping criteria as it should not be stopped before reaching a stable result.

Python Keras Callbacks provides an Early stopping method that allows entering a large number of epochs, and the model training will stop automatically once the model performance stops improving. The loss function is the evaluation parameter to be optimized during the model training, and it is calculated at the end of each epoch.

Once the results are stable and the loss function is not decreasing anymore or the specified maximum number of epochs reached, the early stopping function will stop the training process. The main advantage of this method to avoid model overfitting [82]. A large number of feedforward network configurations were trained, tested, and evaluated. The final ANN model configuration is presented in Table 3.

Table 3. The optimum configuration of the ANN model

Parameter	Value
Validation set	16%
Training & test sets	6 k-folds
Number of neurons in the input layer	6
Number of hidden layers	3
Number of hidden layers 1, 2 and 3	200
Number of neurons in the output layer	1
Number of folding in cross-validation	3
Number of cross-validation repeats	10
Number of epochs	2407 (Early stop tool)
Optimizer	adam
Activation function	ReLU
Loss function	Mean squared error

4.1.3. Model validation

As stated before, the validation dataset splittted manually for the dataset, and the k-fold cross-validation method was used for training and testing due to the data limitation. This was split the available data into three sets, as mentioned in Table 3. The k-fold cross-

validation is a standard procedure for evaluating a machine learning algorithm's performance on a dataset. This procedure works by splitting the limited dataset into k nonoverlapping folds where each fold is used once held back test set while other folds are used as the training dataset. To improve the performance the repeated k-fold cross-validation is used. It simply replicates cross-validation procedures multiple times and computes the average result of all folds across all runs. The calculated mean result is expected to be much closer to the model's true unknown mean performance. Even though this approach is more computationally expensive, it does not waste data and gives an accurate evaluation of the model performance.

After evaluating the model performance and deciding on the model configuration, the model is fitted using the whole dataset (except the validation dataset) to make predictions on unseen data. The ANN model was validated by using the unseen data from the validation dataset to predict the angles and find the true error between the actual and predicted values. Moreover, the model is used to find the optimal angles based on input parameters by feeding the model with targeted energy absorption properties. The developed ANN model was run multiple times to check the accuracy, reliability, and robustness of the predicted optimal hexagonal angle.

4.2. Models results and discussion

4.2.1. Model Performance

The developed ANN model was applied to predict the optimal angle for the hexagonal energy absorption device based on targeted energy absorption performance parameters. It was able to build up a robust relationship between the AE parameters and

the hexagon's angle. In the model parameter tuning phase, it was noticed that a relatively high number of neurons of 200 in each hidden layer and also a high number of epochs (around 2400 for each run) were needed to improve the model accuracy. This high number of neurons and epochs indicates that the relationship between the independent variables and the dependent variable was not straightforward. For this reason, and in addition to the data limitation, building an accurate predictive ANN model was challenging and required hundreds of runs to optimize it. To avoid the overfitting of the model due to the nigh number of epochs and neurons, the dropout function was used. The dropout function is a regularization technique that prevents neural networks from overfitting [83].

The performance of the model was measured based on loss function values using MSE. The configured model was run many times to check its robustness and reliability then it was validated by making predictions from the validation dataset.

Table 5 shows the results of four runs of training and validating the configured ANN model. The validation dataset consists of the EA properties for 6 angles, and the model was used to predict these 6 angles in order to compare the predicted values with the actual values. The lowest training loss achieved was 0.09, with a validation loss of 0.49. The predicted angles and training and validations MSE values for the best-performed model are shown under Prediction 4 in

Table 5 with accuracy between 98.24% and 99.85%. 2407 epochs were required to reach that accuracy. Furthermore, the R^2 values in

Table 5 indicate how accurate the regression model can predict the angle by comparing the predicted and actual angles. This statistic measure of R^2 is used to determine when the model fits the training data and its capability of providing accurate predictions.

It can be seen that all of the R^2 in the 4 predictions between the actual and predicted angles are very high (the highest is 0.998 and the lowest is 0.9929), which proves the efficiency of the model in predicting the angles based on the energy absorption properties.

The developed ANN model provides satisfactory results, which makes it a very useful tool for product design. It can be used as an intelligent engineering design tool where designers can insert any targeted properties to get the optimal desired parameters, as long as the values of these properties are within the range of the experimental dataset. In this case, an optimal angle can be found with high accuracy only within the range of the trained dataset (30°- 85°).

Table 4. Four runs for predicting the angles using properties from the validation dataset

Actual angle	Predictions 1	Predictions 2	Predictions 3	Predictions 4
30	29.86	30.18	29.04	29.51
40	39.78	40.23	38.29	40.28
50	49.22	48.74	49.36	49.28
60	60.38	60.38	60.74	60.74
70	70.06	68.94	68.48	68.77
80	81.75	82.48	82.17	80.12

Table 5. The associated losses and R^2 for each prediction run

	Predictions 1	Predictions 2	Predictions 3	Predictions 4
Training loss	0.4582	0.6126	0.4804	0.0872
Training R^2	0.99913	0.99872	0.9992	0.9997
Validation loss	0.6473	1.5146	1.878	0.4855
Validation R^2	0.9977	0.99480	0.9935	0.9983

4.2.1. Angle predictions

The trained best-performed model was used to predict the angles based on their energy absorption parameters that were calculated from the load-displacement experimental data that resulted from applying the quasi-static compression test on the test specimens. The trained models were saved using Keras 'model. Save ()' function and then loaded with 'load_model()' whenever need to use it for prediction to save time required to run the whole process and also to be able to use the trained model across platforms. The input parameters were typed manually and sent via Keras 'model. predict()' function to predict the angle from unseen data. The predicted angle can be any value between 30° and 85°, including the values in-between the angles used to get the experimental data.

The ANN model was used for geometry optimization by predicting the optimal angle to design a passive hexagonal energy absorption device. Two different sets of targeted properties were used to predict an angle for two different needs or applications. The first will be to maximize the energy absorbed by the hexagonal structure and the failure mechanism's stability by maximizing the crushing force efficiency. The targeted properties in Table 6 will be used to predict the optimal angle to use this structure as an energy absorber in vehicles where the SEA and CFE will be maximized, and the IPF will be the same as the MF ensure stable crushing. It must be noted that the angle predicted here is the optimal angle required to achieve the targeted performance. As seen in Table 6, the predicted optimal angle for the targeted parameters is 48.33°.

The second prediction will be to maximize the load-carrying capacity before crushing is initiated by increasing the initial peak force and energy absorbed in the pre-crushing phase. The targeted performance parameters are as in Table 7, where the predicted

Table 6. Prediction of optimal angle for energy absorption

-	Specific Absorbed Energy SAE [KJ/g]	Pre-crushing Specific Absorbed Energy PRE-SAE [KJ/g]	Post-crushing Specific Absorbed Energy POST-SAE [KJ/g]	Initial Peak Force IPF [N]	Mean Crushing Force MCF [N]	Crushing Force Efficiency CFE	Predicted Optimal Angle
Targeted EA performance parameters	224.62	30.18	194.44	0.19	0.20	1.05	43.43°

Table 7. Prediction of optimal angle for load-carrying capacity

-	Specific Absorbed Energy SAE [KJ/g]	Pre-crushing Specific Absorbed Energy PRE-SAE [KJ/g]	Post-crushing Specific Absorbed Energy POST-SAE [KJ/g]	Initial Peak Force IPF [N]	Mean Crushing Force MCF [N]	Crushing Force Efficiency CFE	Predicted Optimal Angle
Targeted EA performance parameters	578.02	22.63	555.39	0.64	0.37	0.56	73.42°

angle was 73.42°. The proposed strategic procedure in this thesis to predicting the interior angle of a hexagonal structure based on specific properties using the ANN model can be easily be used for different geometries and structures, and even on composites materials compositions, as long as the experimental data of the required mechanical properties are available to the product designers.

CHAPTER 5. CONCLUSION AND RECOMMENDATIONS

In the first stage study, hexagonal structures were subjected to quasi-static axial compression tests to determine the effect of hexagon's interior angel on their crashworthiness properties. These structures are designed to have varying interior angle values (30°-85°) to study the relationship between the angle values and the energy absorption performance indicators. After conducting the test and collecting the load-displacement data used to calculate the total specific energy absorption, the specific energy absorption in the pre-crushing zone, the specific energy absorption in the post-crushing zone, the initial peak force, the mean crushing force, and the crushing force efficiency. These calculated parameters and the recorded crushing footage from the test are used to provide a detailed analysis of the experimental study results. In the second stage of this study, an ANN model was developed to predict optimal hexagonal ring angle based on targeted EA indicators. The experimental data are used as an input dataset to train, test, and validate the ANN model to be used as a predictive model that can provide accurate predictions. The feedforward ANN was used with the backpropagation of the error training algorithm. The mean squared error value was used as the loss function, and the k-fold cross-validation method was used to evaluate the model's performance. Lastly, the final predictive model was trained on the entire dataset, saved, and made ready to make predictions based on any targeted energy absorption performance.

5.1. Conclusion

The following conclusions were drawn from the study:

- The energy absorption performance significantly varies depending on the interior hexagonal angle value.

- From the load-displacement curves, it was noticed the smaller angles (30°-55°) showed a very stable crushing mechanism under the compression test with lower IPF. These angles also achieved a higher CFE than the larger angles where the best CFE reported was for angles 40° and 45° at 1.03 and 0.97, respectively.
- The larger angles showed a significant decrease in the load-carrying capacity after reaching the initial peak force, which caused the CFE to be reduced. The lowest CFE was for angle 85° at only 22%. While the most energy absorbed was by angle 75°.
- All of the energy performance indicators are plotted against the angle to get an insight into the relationship between them. From the plots, the relationship was highly non-linear, making the optimization of the interior angle of the hexagonal structure a complex task.
- The developed model was validated by using it to predict the angles from the unseen validation dataset. The model's performance exceeded the required accuracy specified in the thesis objectives and predicted the angles with an accuracy between 98.24% and 99.85%.
- Finally, the model is used to predict the optimal angle based on two cases of targeted EA properties. The first was to maximize energy absorbed and the CFE while minimizing IPF and make it closer to the MF to ensure stable crushing; the predicted optimal angle was 43.43°. The second case was to maximize the load-carrying capacity before the crushing was initiated by increasing the IPF

and the amount of energy absorbed in the pre-crushing phase. The model predicted that angle 73.42° would be best suited for the targeted properties.

5.2. Recommendations for Future Work

For future work, it is recommended to investigate the accuracy of the predictions through fabricating new structures with the predicted optimal interior angles and test them under quasi-static compression test to obtain the actual energy absorption performance indicators and compare them with the targeted indicators which were fed into the trained ANN model to make the predictions. This comparison will provide further insight into the model's performance.

It would be very beneficial to perform a study on the required amount of experimental data required to accurately optimize a certain design parameter. This could save the time and money required to conduct a large number of tests for optimization and help in efficient experiment planning. Furthermore, more features and mechanical properties should be investigated as there might be other features that have a more direct relationship with the predicted/optimized structure's angle, which can make the ANN model simpler and more accurate. Lastly, it is recommended to investigate how the proposed approach can be used to develop the ANN model and use it for multi-objective optimization where more than one design parameter can be optimized simultaneously.

REFERENCES

[1] Z. Fan, G. Lu, and K. Liu, “Quasi-static axial compression of thin-walled tubes with different cross-sectional shapes,” *Eng. Struct.*, vol. 55, pp. 80–89, 2013, doi: 10.1016/j.engstruct.2011.09.020.

[2] D. Karagiozova, G. N. Nurick, and S. Chung Kim Yuen, “Energy absorption of aluminum alloy circular and square tubes under an axial explosive load,” *Thin-Walled Struct.*, vol. 43, no. 6, pp. 956–982, 2005, doi: 10.1016/j.tws.2004.11.002.

[3] C. Baykasoglu and M. T. Cetin, “Energy absorption of circular aluminum tubes with functionally graded thickness under axial impact loading,” *Int. J. Crashworthiness*, vol. 20, no. 1, pp. 95–106, 2015, doi: 10.1080/13588265.2014.982269.

[4] H. Wang, M. Su, and H. Hao, “The quasi-static axial compressive properties and energy absorption behavior of ex-situ ordered aluminum cellular structure filled tubes,” *Compos. Struct.*, vol. 239, p. 112039, 2020, doi: 10.1016/j.compstruct.2020.112039.

[5] M. Kathiresan, “Influence of shape, size and location of cutouts on crashworthiness performance of aluminum conical frusta under quasi-static axial compression,” *Thin-Walled Struct.*, vol. 154, no. May, p. 106793, 2020, doi: 10.1016/j.tws.2020.106793.

[6] A. P. Meran, C. Baykasoglu, A. Mugan, and T. Toprak, “Development of a design for a crash energy management system for use in a railway passenger car,” *Proc. Inst. Mech. Eng. Part F J. Rail Rapid Transit*, vol. 230, no. 1, pp. 206–219, 2016, doi: 10.1177/0954409714533321.

[7] S. R. Guillow, G. Lu, and R. H. Grzebieta, “Quasi-static axial compression of thin-

walled circular aluminum tubes," *Int. J. Mech. Sci.*, vol. 43, no. 9, pp. 2103–2123, 2001, doi: 10.1016/S0020-7403(01)00031-5.

[8] X. Zhang and H. Huh, "Crushing analysis of polygonal columns and angle elements," *Int. J. Impact Eng.*, vol. 37, no. 4, pp. 441–451, 2010, doi: 10.1016/j.ijimpeng.2009.06.009.

[9] K. S. Lee, S. K. Kim, and I. Y. Yang, "The energy absorption control characteristics of Al thin-walled tube under quasi-static axial compression," *J. Mater. Process. Technol.*, vol. 201, no. 1–3, pp. 445–449, 2008, doi: 10.1016/j.jmatprotec.2007.11.155.

[10] S. Gowid, E. Mahdi, and F. Alabtah, "Modeling and optimization of the crushing behavior and energy absorption of plain weave composite hexagonal quadruple ring systems using artificial neural network," *Compos. Struct.*, vol. 229, no. July, p. 111473, 2019, doi: 10.1016/j.compstruct.2019.111473.

[11] X. Luo, J. Xu, J. Zhu, Y. Gao, L. Nie, and W. Li, "A new method to investigate the energy absorption characteristics of thin-walled metal circular tube using finite element analysis," *Thin-Walled Struct.*, vol. 95, pp. 24–30, 2015, doi: 10.1016/j.tws.2015.06.001.

[12] A. Esnaola, B. Elguezabal, J. Aurrekoetxea, I. Gallego, and I. Ulacia, "Optimization of the semi-hexagonal geometry of a composite crush structure by finite element analysis," *Compos. Part B Eng.*, vol. 93, pp. 56–66, 2016, doi: 10.1016/j.compositesb.2016.03.002.

[13] L. Aktay, B. H. Kröplin, A. K. Toksoy, and M. Güden, "Finite element and coupled finite element/smooth particle hydrodynamics modeling of the quasi-static crushing

of empty and foam-filled single, tubular and constraint hexagonal- and square-packed aluminum tubes," *Mater. Des.*, vol. 29, no. 5, pp. 952–962, 2008, doi: 10.1016/j.matdes.2007.03.019.

[14] S. Gangi Setti and R. N. Rao, "Artificial neural network approach for prediction of stress-strain curve of near β titanium alloy," *Rare Met.*, vol. 33, no. 3, pp. 249–257, 2014, doi: 10.1007/s12598-013-0182-2.

[15] M. I. Khan, "Predicting properties of High Performance Concrete containing composite cementitious materials using Artificial Neural Networks," in *Automation in Construction*, 2012, vol. 22, doi: 10.1016/j.autcon.2011.11.011.

[16] X. Li, Z. Liu, S. Cui, C. Luo, C. Li, and Z. Zhuang, "Predicting the effective mechanical property of heterogeneous materials by image-based modeling and deep learning," *Comput. Methods Appl. Mech. Eng.*, vol. 347, 2019, doi: 10.1016/j.cma.2019.01.005.

[17] A. Afram, F. Janabi-Sharifi, A. S. Fung, and K. Raahemifar, "Artificial neural network (ANN) based model predictive control (MPC) and optimization of HVAC systems: A state of the art review and case study of a residential HVAC system," *Energy Build.*, vol. 141, 2017, doi: 10.1016/j.enbuild.2017.02.012.

[18] T. Zarra, M. G. Galang, F. Ballesteros, V. Belgiorno, and V. Naddeo, "Environmental odor management by artificial neural network – A review," *Environment International*, vol. 133. 2019, doi: 10.1016/j.envint.2019.105189.

[19] E. S. Mahdi and H. El-Kadi, "Crushing behavior of laterally compressed composite elliptical tubes: Experiments and predictions using artificial neural networks," *Compos. Struct.*, vol. 83, no. 4, pp. 399–412, 2008, doi:

10.1016/j.compstruct.2007.05.009.

[20] O. Laban, S. Gowid, and E. Mahdi, “Experimental Investigation and Uncertainty Prediction of the Load-Carrying Capacity of Composite Double Hat for Lattice Core Sandwich Panels Using Artificial Neural Network,” 2020, doi: 10.1109/ICIoT48696.2020.9089603.

[21] M. Zakaulla, F. Parveen, Amreen, Harish, and N. Ahmad, “Artificial neural network-based prediction on tribological properties of polycarbonate composites reinforced with graphene and boron carbide particle,” in *Materials Today: Proceedings*, 2019, vol. 26, doi: 10.1016/j.matpr.2019.11.276.

[22] T. G. Clarkson, “Introduction to neural networks,” *Neural Netw. World*, vol. 6, no. 2, 1996, doi: 10.1201/9781482277180-13.

[23] V. Patel, G. Tiwari, and R. Dumpala, “Review of the crushing response of collapsible tubular structures,” *Front. Mech. Eng.*, vol. 15, no. 3, pp. 438–474, 2020, doi: 10.1007/s11465-019-0579-1.

[24] M. R. Nurul Fazita, H. P. S. Abdul Khalil, A. Nor Amira Izzati, and S. Rizal, “Effects of strain rate on failure mechanisms and energy absorption in polymer composites,” in *Failure Analysis in Biocomposites, Fibre-Reinforced Composites and Hybrid Composites*, 2018.

[25] J. J. Carruthers, A. P. Kettle, and A. M. Robinson, “Energy absorption capability and crashworthiness of composite material structures: A review,” *Appl. Mech. Rev.*, vol. 51, no. 10, pp. 635–649, 1998, doi: 10.1115/1.3100758.

[26] R. A. Eshkoor, S. A. Oshkovr, A. B. Sulong, R. Zulkifli, A. K. Ariffin, and C. H. Azhari, “Comparative research on the crashworthiness characteristics of woven

natural silk/epoxy composite tubes," *Mater. Des.*, vol. 47, 2013, doi: 10.1016/j.matdes.2012.11.030.

[27] E. Mahdi, A. M. S. Hamouda, and T. A. Sebaey, "The effect of fiber orientation on the energy absorption capability of axially crushed composite tubes," *Mater. Des.*, vol. 56, 2014, doi: 10.1016/j.matdes.2013.12.009.

[28] A. Alavi Nia and M. Parsapour, "Comparative analysis of energy absorption capacity of simple and multi-cell thin-walled tubes with triangular, square, hexagonal and octagonal sections," *Thin-Walled Struct.*, vol. 74, pp. 155–165, 2014, doi: 10.1016/j.tws.2013.10.005.

[29] J. M. Alexander, "An approximate analysis of the collapse of thin cylindrical shells under axial loading," *Q. J. Mech. Appl. Math.*, vol. 13, no. 1, 1960, doi: 10.1093/qjmam/13.1.10.

[30] T. Wierzbicki and W. Abramowicz, "on the Crushing Mechanics of Thin-Walled Structures.," *Am. Soc. Mech. Eng.*, no. 83, 1983.

[31] W. Abramowicz and N. Jones, "Dynamic axial crushing of circular tubes," *Int. J. Impact Eng.*, vol. 2, no. 3, pp. 263–281, 1984, doi: 10.1016/0734-743X(84)90010-1.

[32] K. R. F. Andrews, G. L. England, and E. Ghani, "Classification of the axial collapse of cylindrical tubes under quasi-static loading," *Int. J. Mech. Sci.*, vol. 25, no. 9–10, 1983, doi: 10.1016/0020-7403(83)90076-0.

[33] N. K. Gupta and H. Abbas, "Lateral collapse of composite cylindrical tubes between flat platens," *Int. J. Impact Eng.*, vol. 24, no. 4, 2000, doi: 10.1016/S0734-743X(99)00173-6.

[34] A. A. A. Alghamdi, “Collapsible impact energy absorbers: An overview,” *Thin-Walled Struct.*, vol. 39, no. 2, pp. 189–213, 2001, doi: 10.1016/S0263-8231(00)00048-3.

[35] J. A. Deruntz and P. G. Hodge, “Crushing of a tube between rigid plates,” *J. Appl. Mech. Trans. ASME*, vol. 30, no. 3, 1960, doi: 10.1115/1.3636567.

[36] T. Yella Reddy and S. R. Reid, “Lateral compression of tubes and tube-systems with side constraints,” *Int. J. Mech. Sci.*, vol. 21, no. 3, 1979, doi: 10.1016/0020-7403(79)90023-7.

[37] L. Wu and J. F. Carney, “Initial collapse of braced elliptical tubes under lateral compression,” *Int. J. Mech. Sci.*, vol. 39, no. 9, 1997, doi: 10.1016/s0020-7403(97)00004-0.

[38] E. S. Mahdi and H. El-Kadi, “Crushing behavior of laterally compressed composite elliptical tubes: Experiments and predictions using artificial neural networks,” *Compos. Struct.*, vol. 83, no. 4, 2008, doi: 10.1016/j.compstruct.2007.05.009.

[39] V. Patel, G. Tiwari, and R. Dumpala, “Review of the crushing response of collapsible tubular structures,” *Frontiers of Mechanical Engineering*, vol. 15, no. 3. 2020, doi: 10.1007/s11465-019-0579-1.

[40] Y. Chen, C. Qiao, X. Qiu, S. Zhao, C. Zhen, and B. Liu, “A novel self-locked energy absorbing system,” *J. Mech. Phys. Solids*, vol. 87, 2016, doi: 10.1016/j.jmps.2015.11.008.

[41] A. Baroutaji, M. D. Gilchrist, and A. G. Olabi, “Quasi-static, impact and energy absorption of internally nested tubes subjected to lateral loading,” *Thin-Walled Struct.*, vol. 98, 2016, doi: 10.1016/j.tws.2015.10.001.

[42] H. Wang, J. Yang, H. Liu, Y. Sun, and T. X. Yu, “Internally nested circular tube system subjected to lateral impact loading,” *Thin-Walled Struct.*, vol. 91, 2015, doi: 10.1016/j.tws.2015.02.014.

[43] A. G. Olabi, E. Morris, M. S. J. Hashmi, and M. D. Gilchrist, “Optimised design of nested circular tube energy absorbers under lateral impact loading,” *Int. J. Mech. Sci.*, vol. 50, no. 1, 2008, doi: 10.1016/j.ijmecsci.2007.04.005.

[44] F. Tarlochan and S. Ramesh, “Composite sandwich structures with nested inserts for energy absorption application,” *Compos. Struct.*, vol. 94, no. 3, 2012, doi: 10.1016/j.compstruct.2011.10.010.

[45] E. Mahdi and A. M. S. Hamouda, “Energy absorption capability of composite hexagonal ring systems,” *Mater. Des.*, vol. 34, pp. 201–210, 2012, doi: 10.1016/j.matdes.2011.07.070.

[46] S. A. Galehdari, M. Kadkhodayan, and S. Hadidi-Moud, “Low-velocity impact and quasi-static in-plane loading on a graded honeycomb structure; experimental, analytical and numerical study,” *Aerosp. Sci. Technol.*, vol. 47, 2015, doi: 10.1016/j.ast.2015.10.010.

[47] F. Sun, C. Lai, and H. Fan, “In-plane compression behavior and energy absorption of hierarchical triangular lattice structures,” *Mater. Des.*, vol. 100, 2016, doi: 10.1016/j.matdes.2016.03.023.

[48] A. Reyes, M. Langseth, and O. S. Hopperstad, “Crashworthiness of aluminum extrusions subjected to oblique loading: Experiments and numerical analyses,” *Int. J. Mech. Sci.*, vol. 44, no. 9, 2002, doi: 10.1016/S0020-7403(02)00050-4.

[49] I. Duarte, M. Vesenjak, and L. Krstulović-Opara, “Dynamic and quasi-static

bending behavior of thin-walled aluminum tubes filled with aluminum foam," *Compos. Struct.*, vol. 109, no. 1, 2014, doi: 10.1016/j.compstruct.2013.10.040.

[50] A. Asanjarani, A. Mahdian, and S. H. Dibajian, "Comparative analysis of energy absorption behavior of tapered and grooved thin-walled tubes with the various geometry of the cross-section," *Mech. Adv. Mater. Struct.*, vol. 27, no. 8, pp. 633–644, 2020, doi: 10.1080/15376494.2018.1488311.

[51] H. S. Kim, "New extruded multi-cell aluminum profile for maximum crash energy absorption and weight efficiency," *Thin-Walled Struct.*, vol. 40, no. 4, 2002, doi: 10.1016/S0263-8231(01)00069-6.

[52] S. Lee, C. Hahn, M. Rhee, and J. E. Oh, "Effect of triggering on the energy absorption capacity of axially compressed aluminum tubes," *Mater. Des.*, vol. 20, no. 1, 1999, doi: 10.1016/s0261-3069(98)00043-0.

[53] K. C. Shin, J. J. Lee, K. H. Kim, M. C. Song, and J. S. Huh, "Axial crush and bending collapse of an aluminum/GFRP hybrid square tube and its energy absorption capability," *Compos. Struct.*, vol. 57, no. 1–4, 2002, doi: 10.1016/S0263-8223(02)00094-6.

[54] H. Kavi, A. K. Toksoy, and M. Guden, "Predicting energy absorption in a foam-filled thin-walled aluminum tube based on experimentally determined strengthening coefficient," *Mater. Des.*, vol. 27, no. 4, 2006, doi: 10.1016/j.matdes.2004.10.024.

[55] T. Miyoshi *et al.*, "Enhancement of energy absorption in a closed-cell aluminum by the modification of cellular structures," *Scr. Mater.*, vol. 41, no. 10, 1999, doi: 10.1016/S1359-6462(99)00255-9.

[56] Q. Liu, J. Ma, Z. He, Z. Hu, and D. Hui, "Energy absorption of bio-inspired multi-

cell CFRP and aluminum square tubes," *Compos. Part B Eng.*, vol. 121, 2017, doi: 10.1016/j.compositesb.2017.03.034.

[57] E. Demirci and A. R. Yildiz, "An investigation of the crash performance of magnesium, aluminum, and advanced high strength steels and different cross-sections for vehicle thin-walled energy absorbers," *Mater. Test.*, vol. 60, no. 7–8, 2018, doi: 10.3139/120.111201.

[58] S. Li, X. Guo, Q. Li, D. Ruan, and G. Sun, "On lateral compression of circular aluminum, CFRP and GFRP tubes," *Compos. Struct.*, vol. 232, 2020, doi: 10.1016/j.compstruct.2019.111534.

[59] Y. Liu, "Crashworthiness design of multi-corner thin-walled columns," *Thin-Walled Struct.*, vol. 46, no. 12, 2008, doi: 10.1016/j.tws.2008.04.003.

[60] A. Niknejad and D. M. Rahmani, "Experimental and theoretical study of the lateral compression process on the empty and foam-filled hexagonal columns," *Mater. Des.*, vol. 53, 2014, doi: 10.1016/j.matdes.2013.06.077.

[61] M. F. M. Alkbir, S. M. Sapuan, A. A. Nuraini, and M. R. Ishak, "Effect of geometry on crashworthiness parameters of natural kenaf fiber-reinforced composite hexagonal tubes," *Mater. Des.*, vol. 60, pp. 85–93, 2014, doi: 10.1016/j.matdes.2014.02.031.

[62] W. Li, Y. Luo, M. Li, F. Sun, and H. Fan, "A more weight-efficient hierarchical hexagonal multi-cell tubular absorber," *Int. J. Mech. Sci.*, vol. 140, 2018, doi: 10.1016/j.ijmecsci.2018.03.006.

[63] Y. Liu, T. A. Schaedler, A. J. Jacobsen, and X. Chen, "Quasi-static energy absorption of hollow micro lattice structures," *Compos. Part B Eng.*, vol. 67, 2014,

doi: 10.1016/j.compositesb.2014.06.024.

[64] A. Esnaola, I. Ulacia, L. Aretxabaleta, J. Aurrekoetxea, and I. Gallego, “Quasi-static crush energy absorption capability of E-glass/polyester and hybrid E-glass-basalt/polyester composite structures,” *Mater. Des.*, vol. 76, 2015, doi: 10.1016/j.matdes.2015.03.044.

[65] R. Shams, A. Niknejad, A. G. Olabi, and M. Z. Nejad, “Quasi-static flattening energy absorption process on preformed circular tubes by numerical and experimental analyses,” *Thin-Walled Struct.*, vol. 144, 2019, doi: 10.1016/j.tws.2019.106260.

[66] J. Ma, H. Dai, M. Shi, L. Yuan, Y. Chen, and Z. You, “Quasi-static axial crushing of hexagonal origami crash boxes as energy absorption devices,” *Mech. Sci.*, vol. 10, no. 1, 2019, doi: 10.5194/ms-10-133-2019.

[67] S. Linforth, T. Ngo, P. Tran, D. Ruan, and R. Odish, “Investigation of the auxetic oval structure for energy absorption through quasi-static and dynamic experiments,” *Int. J. Impact Eng.*, vol. 147, 2021, doi: 10.1016/j.ijimpeng.2020.103741.

[68] M. S. Abu Bakar, M. S. Salit, M. Z. Mohamad Yusoff, E. S. Zainudin, and H. H. Ya, “The crashworthiness performance of stacking sequence on filament-wound hybrid composite energy absorption tube subjected to quasi-static compression load,” *J. Mater. Res. Technol.*, vol. 9, no. 1, 2020, doi: 10.1016/j.jmrt.2019.11.006.

[69] M. Alkateb, S. M. Sapuan, Z. Leman, M. Jawaid, and M. R. Ishak, “Quasi-static crush behavior of environmentally friendly kenaf/wool epoxy composites elliptical tube,” *J. Mech. Eng. Sci.*, vol. 12, no. 2, 2018, doi: 10.15282/jmes.12.2.2018.13.0325.

[70] Y. Xiang, T. Yu, and L. Yang, “Comparative analysis of energy absorption capacity of polygonal tubes, multi-cell tubes, and honeycombs by utilizing key performance indicators,” *Mater. Des.*, vol. 89, pp. 689–696, 2016, doi: 10.1016/j.matdes.2015.10.004.

[71] S. E. Alkhatib, M. S. Matar, F. Tarlochan, O. Laban, A. S. Mohamed, and N. Alqwasmi, “Deformation modes and crashworthiness energy absorption of sinusoidally corrugated tubes manufactured by direct metal laser sintering,” *Eng. Struct.*, vol. 201, 2019, doi: 10.1016/j.engstruct.2019.109838.

[72] X. Cao, S. Duan, J. Liang, W. Wen, and D. Fang, “Mechanical properties of an improved 3D-printed rhombic dodecahedron stainless steel lattice structure of variable cross-section,” *Int. J. Mech. Sci.*, vol. 145, 2018, doi: 10.1016/j.ijmecsci.2018.07.006.

[73] M. Y. Rafiq, G. Bugmann, and D. J. Easterbrook, “Neural network design for engineering applications,” *Comput. Struct.*, vol. 79, no. 17, pp. 1541–1552, 2001, doi: 10.1016/S0045-7949(01)00039-6.

[74] I. Flood, “A Neural Network Approach to the Sequencing of Construction Tasks,” 2017, doi: 10.22260/isarc1989/0026.

[75] H. Rahmanpanah, S. Mouloodi, C. Burvill, S. Gohari, and H. M. S. Davies, “Prediction of load-displacement curve in a complex structure using artificial neural networks: A study on a long bone,” *Int. J. Eng. Sci.*, vol. 154, 2020, doi: 10.1016/j.ijengsci.2020.103319.

[76] P. G. Benardos and G. C. Vosniakos, “Optimizing feedforward artificial neural network architecture,” *Eng. Appl. Artif. Intell.*, vol. 20, no. 3, 2007, doi:

10.1016/j.engappai.2006.06.005.

[77] D. Wu and G. G. Wang, “Causal artificial neural network and its applications in engineering design,” *Eng. Appl. Artif. Intell.*, vol. 97, no. August 2019, 2021, doi: 10.1016/j.engappai.2020.104089.

[78] H. Zhang and J.-H. Mu, “A Back Propagation Neural Network-Based Method for Intelligent Decision-Making,” *Complexity*, vol. 2021, 2021, doi: 10.1155/2021/6610797.

[79] N. Srivastava, G. Hinton, A. Krizhevsky, I. Sutskever, and R. Salakhutdinov, “Dropout: A simple way to prevent neural networks from overfitting,” *J. Mach. Learn. Res.*, vol. 15, 2014.

[80] M. K. Kazi, F. Eljack, and E. Mahdi, “Predictive ANN models for varying filler content for cotton fiber/PVC composites based on experimental load-displacement curves,” *Compos. Struct.*, vol. 254, no. August, p. 112885, 2020, doi: 10.1016/j.compstruct.2020.112885.

[81] Keras, “Dense layer,” *https://Keras.Io/Api/Layers/Core_Layers/Dense/*. 2020.

[82] Keras, “EarlyStopping.” *https://keras.io/api/callbacks/early_stopping/.*

[83] “Dropout_Layer.” *https://keras.io/api/layers/regularization_layers/dropout/*